



Swansea University  
Prifysgol Abertawe



## Cronfa - Swansea University Open Access Repository

---

This is an author produced version of a paper published in:  
*Quaternary Research*

Cronfa URL for this paper:  
<http://cronfa.swan.ac.uk/Record/cronfa51099>

---

### **Paper:**

Matthews, J., Wilson, P., Winkler, S., Mourné, R., Hill, J., Owen, G., Hiemstra, J., Hallang, H. & Geary, A. (2019). Age and development of active cryoplanation terraces in the alpine permafrost zone at Svartkampan, Jotunheimen, southern Norway. *Quaternary Research*, 1-24.  
<http://dx.doi.org/10.1017/qua.2019.41>

Released under the terms of a Creative Commons Attribution Non-Commercial No Derivatives License (CC-BY-NC-ND).

---

This item is brought to you by Swansea University. Any person downloading material is agreeing to abide by the terms of the repository licence. Copies of full text items may be used or reproduced in any format or medium, without prior permission for personal research or study, educational or non-commercial purposes only. The copyright for any work remains with the original author unless otherwise specified. The full-text must not be sold in any format or medium without the formal permission of the copyright holder.

Permission for multiple reproductions should be obtained from the original author.

Authors are personally responsible for adhering to copyright and publisher restrictions when uploading content to the repository.

<http://www.swansea.ac.uk/library/researchsupport/ris-support/>

1 **Age and development of active cryoplanation terraces in the alpine permafrost**  
2 **zone at Svartkampan, Jotunheimen, southern Norway**

3

4 John A. Matthews<sup>1</sup>, Peter Wilson<sup>2</sup>, Stefan Winkler<sup>3</sup>, Richard W. Mourné<sup>4</sup>, Jennifer L.  
5 Hill<sup>4</sup>, Geraint Owen<sup>1</sup>, John F. Hiemstra<sup>1</sup>, Helen Hallang<sup>1</sup> and Andrew P. Geary<sup>4</sup>

6

7 <sup>1</sup> Department of Geography, College of Science, Swansea University, Singleton Park,  
8 Swansea SA2 8PP, Wales, UK

9

10 <sup>2</sup> School of Geography and Environmental Sciences, Ulster University, Cromore  
11 Road, Coleraine BT52 1SA, Northern Ireland, UK

12

13 <sup>3</sup> Department of Geography and Geology, Julius-Maximilians University Würzburg,  
14 Am Hubland, Würzburg 97070, Germany

15

16 <sup>4</sup> Department of Geography and Environmental Management, University of the West  
17 of England, Coldharbour Lane, Bristol BS16 1QY, UK

18

19 **Correspondence to:**

20 John A. Matthews, Department of Geography, College of Science, Swansea  
21 University, Singleton Park, Swansea SA2 8PP, Wales, UK

22 E-mail: [J.A.Matthews@Swansea.ac.uk](mailto:J.A.Matthews@Swansea.ac.uk)

23 Telephone: +44 1633 413291

24

25

26 **ABSTRACT**

27

28 Schmidt-hammer exposure-age dating (SHD) of boulders on cryoplanation terrace treads and  
29 associated bedrock cliff faces revealed Holocene ages ranging from  $0 \pm 825$  to  $8890 \pm 1185$   
30 yr. The cliffs were significantly younger than the inner treads, which tended to be younger  
31 than the outer treads. Radiocarbon dates from the regolith of 3854 to 4821 cal yr BP ( $2\sigma$   
32 range) indicated maximum rates of cliff recession of  $\sim 0.1$  mm/year, which suggests the onset of  
33 terrace formation prior to the last glacial maximum. Age, angularity and size of clasts, together  
34 with planation across bedrock structures and the seepage of groundwater from the cliff foot, all  
35 support a process-based conceptual model of cryoplanation terrace development in which frost  
36 weathering leads to parallel cliff recession and hence terrace extension. The availability of  
37 groundwater during autumn freeze-back is viewed as critical for frost wedging and/or the  
38 growth of segregation ice during prolonged winter frost penetration. Permafrost promotes  
39 cryoplanation by providing an impermeable frost table beneath the active layer, focusing  
40 groundwater flow, and supplying water for sediment transport by solifluction across the tread.  
41 Snowbeds are considered an effect rather than a cause of cryoplanation terraces and  
42 cryoplanation is seen as distinct from nivation.

43

44 **KEY WORDS**

45

46 cryoplanation terraces, Schmidt-hammer exposure-age dating, mountain permafrost,  
47 periglacial processes, alpine landform development, frost weathering, nivation.

48

49 **INTRODUCTION**

50

51 Cryoplanation terraces (also known as altiplanation or goletz terraces and by several  
52 other terms) are periglacial landforms consisting of nearly horizontal bedrock surfaces

53 or benches, backed by frost-weathered bedrock cliffs (Demek, 1969a; Washburn, 1979;  
54 Ballantyne, 2018; French, 2018; Harris et al., 2018). The terraces are typically tens of  
55 metres wide and hundreds of metres long, with a thin cover of regolith. They may occur  
56 singly or as an altitudinal sequence of hillslope ‘steps’ that sometimes culminate in  
57 ‘summit flats’ (Czudek, 1995; Lauriol et al., 2006; Křížek, 2007; Hall and André, 2010;  
58 Nelson and Nyland, 2017).

59

60 Cryoplanation terraces are generally supposed to have developed by processes  
61 of ‘cryoplanation’ – commonly interpreted to include a combination of frost weathering  
62 on bedrock cliffs and the removal of the weathered debris by solifluction and/or flowing  
63 water – resulting in cliff recession and terrace extension (Boch and Krasnov, 1943;  
64 Demek, 1969b; Priesnitz, 1988; Lauriol, 1990; Ballantyne, 2018). Indeed, Schunke  
65 (1977) suggested that cryoplanation terraces may be the only meso-scale landforms that  
66 can be used to characterise the periglacial zone, and hence define a truly periglacial  
67 environment. The processes of cryoplanation also underpin attempts to define  
68 distinctive models of periglacial hillslope and landscape evolution (cf. Peltier, 1950;  
69 Richter et al., 1963; French, 2016).

70

71 However, although cryoplanation terraces have been widely recognised in  
72 regions with present or former non-glacial cold climates, such as Siberia (Boch and  
73 Krasnov, 1943, Demek, 1968; Czudek, 1995), Mongolia (Richter et al., 1963); Alaska  
74 (Reger and Péwé, 1976, Nelson, 1998; Nelson and Nyland, 2017), Northern Canada  
75 (Lauriol and Godbout, 1988; Lauriol et al., 2006), Central Europe (Demek, 1969a;  
76 Traczyk and Migon, 2000; Křížek, 2007), Iceland (Schunke and Heckendorff, 1976;  
77 Schunke, 1977), the Andes (Grosso and Corte, 1991), Antarctica (Hall, 1997; Hall and

78 André, 2010) and the British Isles (Te Punga, 1956; Waters, 1962), criteria for the  
79 recognition of active features are largely lacking. In the absence of dating evidence,  
80 moreover, most examples discussed in the literature are of unknown age and many are  
81 regarded as relict. Furthermore, there is disagreement over the necessary climatic  
82 conditions under which cryoplanation terraces can form, and whether cryoplanation  
83 terraces are characteristic of permafrost environments, as advocated by Reger and Pewe  
84 (1976) or can also form under climatic regimes characterised only by seasonal frost  
85 (Demek, 1969a).

86

87         The precise processes constituting cryoplanation, the rate of development of  
88 cryoplanation terraces, their status as palaeoclimatic indicators, and their role in the  
89 evolution of periglacial landscapes, all remain highly controversial topics. Furthermore,  
90 as cryoplanation terraces are often the sites of long-lasting snowbeds, this has led to the  
91 suggestion that cryoplanation is essentially similar to ‘nivation’ – the suite of  
92 weathering and transport processes that may be enhanced by the presence of late-lying  
93 or perennial snow – which is another problematic subject (St-Onge, 1964, 1969; Hall,  
94 1998; Thorn and Hall, 2002; Margold et al., 2011; Rixhon and Demoulin, 2013).

95 Arguably, despite the recent research from the Antarctic, there has been little progress  
96 in understanding cryoplanation terraces since the definitive monograph of Demek  
97 (1969a): new insights are therefore long overdue.

98

99         This paper presents the results of an investigation of active cryoplanation  
100 terraces recently discovered at Svartkampan in the permafrost zone of NE Jotunheimen,  
101 alpine southern Norway. These landforms are believed to be the first active  
102 cryoplanation terraces to be recognised as such in Norway and have the potential to

103 resolve several of the aforementioned controversies regarding the nature and  
104 significance of cryoplanation and related topics. Our specific objectives are as follows:

105

- 106 1. To describe the morphology of the proposed cryoplanation terraces.
- 107 2. To date the terraces using Schmidt-hammer exposure-age dating (SHD),  
108 complemented by radiocarbon dating, and hence provide firm evidence of landform age  
109 and present levels of activity.
- 110 3. To assess observational evidence of the environmental controls on terrace  
111 formation at the site, including geological structure, climate, permafrost, snow, and  
112 groundwater hydrology.
- 113 4. To test current ideas on cryoplanation processes in the light of the new evidence  
114 from Svartkampan, and propose a process-based conceptual model of cryoplanation  
115 terrace development.

116

## 117 **LOCATION AND ENVIRONMENT**

118

119 Svartkampan is a spur located on the northern slope of the Galdhøpiggen massif of  
120 northeastern Jotunheimen, the highest mountains in Norway (Figure 1). The  
121 cryoplanation terraces (sites 1-10) occur as a series of north-facing steps with backing  
122 cliffs cut into bedrock at an altitude of 1540-1575 m above sea level (Figures 1c and  
123 2a). These terraces sit on the northern rim of Juvflye, a high-altitude plateau, where  
124 related forms have been mapped as perennial snowbeds but not as cryoplanation  
125 terraces (Ødegård et al., 1987). The study sites lies at least 500 m above the tree line:  
126 close to the upper altitudinal limit of the mid-alpine belt, which occurs locally at ~1600  
127 m (Matthews et al., 2018a; see also, NIJOS, 1991). Extensive areas of active and relict

128 periglacial patterned ground (sorted circles, garlands and stripes) characterise the  
129 largely till-covered landscape at and above the altitude of the sites (Ødegård et al.,  
130 1987, 1988; Winkler et al., 2016) where bedrock outcrops are relatively rare. Beneath  
131 the bedrock cliffs, the treads of the cryoplanation terraces have a similar surface cover  
132 of regolith with an extensive pavement of boulders and cobbles, disturbed soils and a  
133 sparse vegetation cover (Figure 2b).

134

135         Most of the study area is composed of pyroxene-granulite gneiss (Lutro and  
136 Tveten, 1996) but the location of the terraces coincides with a shear zone within the  
137 gneiss. Observations from the backing cliffs of the terraces show that this zone consists  
138 mainly of alternating flaggy layers of varied lithologies including fine-grained black to  
139 dark green mylonite and coarser-grained grey, sheared gneiss. Both lithologies have  
140 lozenge-shaped rotated feldspar crystals and larger pods (>5 cm) of relatively unshredded  
141 but rotated gneiss. Also present are rounded feldspar crystals (typically 1-2 cm), which  
142 give a ‘pebbly’ appearance resembling augen gneiss, white quartz-feldspar layers  
143 (possibly pre-deformational), and occasional larger intrusions of peridotite, which  
144 weathers to a distinctive orange-brown colour. Although not very common at the main  
145 terrace (sites 1-8) and the upper terraces (sites 9 and 10), the ‘pebbly’ gneiss  
146 predominates at another prominent terrace located below and to the north-west of the  
147 main terrace at 1525 m a.s.l.

148

149         Mean annual air temperature (MAAT) estimated from boreholes near the study  
150 site at 1560 m a.s.l., where permafrost is present, is  $-2^{\circ}\text{C}$  with a mean July air  
151 temperature of  $+5^{\circ}\text{C}$  and a mean January air temperature of  $-8^{\circ}\text{C}$  (Farbrot et al., 2011;  
152 Lilleøren et al., 2012). These temperature data are consistent with the earlier estimate of

153 -2.6 °C for MAAT at 1500 m a.s.l. interpolated from MAAT measurements at 11  
154 meteorological stations around Jotunheimen (Ødegård et al., 1992). Annual snow depth  
155 is 1.0-1.5 m ([www.se.norge.no/](http://www.se.norge.no/)), while mean annual precipitation (MAP) is 800-1000  
156 mm (Isaksen et al., 2011) with a late-summer maximum characteristic of the continental  
157 climatic regime of eastern Norway. However, strong winds on Juvflye result in  
158 comparatively little snow cover and a late maximum snow depth of only 0.5 m in May  
159 (Ødegård et al., 1992): our study sites in a leeward position will accumulate  
160 significantly higher values than this.

161

162 Permafrost is widespread in this area of Jotunheimen, where the lower limit of  
163 discontinuous permafrost lies at ~1450 m a.s.l. (Ødegård et al., 1996; Isaksen et al.,  
164 2002; Harris, et al. 2009; Farbroten et al., 2011) and active-layer thickness may be up to 5  
165 m at 1600 m a.s.l. (Hipp et al., 2014). However, the lower limit of permafrost in alpine  
166 rock walls in the area is highly dependent on aspect and is likely to descend to at least  
167 1300 m a.s.l. where these face north (Hipp et al., 2014), possibly within the range 1250-  
168 1400 m a.s.l. (Steiger et al., 2016). There can be no doubt, therefore, that the bedrock  
169 cliffs characterising the cryoplanation terraces at Svartkampan are underlain by  
170 permafrost. Permafrost is likely to have existed throughout the Holocene at altitudes  
171 >1600 m a.s.l. in the study area (Lilleøren et al., 2012). At the slightly lower altitude of  
172 the study sites, therefore, permafrost could have been absent during the Holocene  
173 thermal maximum of the early Holocene, although it may well have survived in the  
174 north-facing bedrock cliffs. The lowest permafrost limits of the Holocene seem to have  
175 occurred during the 'Little Ice Age' (Lilleøren et al., 2012), when MAAT was ~1.0 °C  
176 lower than in AD 1960-1990 (Nesje et al., 2008).

177



178           At the maximum of the last (Weichselian) glaciation, the highest areas of  
179 Jotunheimen were located close to the main ice divide and ice accumulation area of the  
180 Scandinavian ice sheet. Deglaciation is considered to have occurred in the early  
181 Holocene by 9.7 ka, following the Preboreal Erdalen event (cf. Dahl et al., 2002;  
182 Matthews and Dresser, 2008). This conventional interpretation is consistent with basal  
183 radiocarbon dates obtained from peat bogs and lakes from the valleys surrounding the  
184 Galdhøpiggen massif (Barnett et al., 2000; Nesje and Dahl, 2001; Matthews et al., 2005,  
185 2018b; Hormes et al., 2009), empirical evidence of deglaciation elsewhere in southern  
186 Norway and broad-scale reconstruction of the Scandinavian ice-sheet deglaciation  
187 (Goehring et al., 2008; Nesje, 2009; Mangerud et al., 2011; Hughes et al., 2016;  
188 Stroeven et al., 2016; Marr et al., 2018).

189

## 190 **METHODOLOGY**

191

192 Observations and measurements were made at 10 sites on three cryoplanation terraces  
193 (Figures 1c and 3). Cross-profiles of the terrace tread and backing cliff were measured  
194 at each site to define the overall terrace morphology, using a 30-m tape and Abney level  
195 between breaks of slope. Two excavations were made in the tread of the main terrace  
196 (where the boulder cover was least extensive) to examine the subsurface, particularly  
197 the bedrock profile beneath the regolith cover.

198

199           At each site, a total of 300 Schmidt-hammer R-values were measured,  
200 including: 100 boulders each from the inner and outer halves of the tread (one impact  
201 per boulder), and a sample of 100 impacts from the backing cliff (impacts widely  
202 spaced across the cliff face). A mechanical N-type Schmidt hammer (Proceq, 2004) was

203 used throughout and periodically tested on the manufacturer's test anvil to ensure no  
204 deterioration in performance following a large number of impacts (cf. McCarroll, 1987,  
205 1994). Schmidt-hammer measurements were restricted to boulders or bedrock of the  
206 dominant local lithology, namely mylonitised pyroxene-granulite gneiss. Unstable or  
207 small boulders were avoided, as were boulder or bedrock edges, joints or cracks, and  
208 lichen-covered or wet surfaces (cf. Shakesby et al., 2006; Viles et al., 2011; Matthews  
209 and Owen, 2016).

210

211 High-resolution, calibrated-age, Schmidt-hammer exposure-age dating (SHD)  
212 techniques followed the approach developed by Matthews and Owen, (2010), Matthews  
213 and Winkler (2011) and Matthews and McEwen (2013). The approach is based on  
214 establishing a local, linear calibration equation relating mean Schmidt-hammer R-value  
215 to rock-surface exposure age based on two surfaces of known age ('old' and 'young'  
216 control points). The control points used in this study relate to the local mylonitised  
217 pyroxene-granulite gneiss. The 'old' control point, which is located within 200 m of the  
218 western end of the main terrace (M in Figure 1c), consists of glacially-scoured bedrock  
219 surfaces. The age of 9.7 ka assigned to these surfaces is the conventional age of  
220 deglaciation in central Jotunheimen (Matthews et al., 2018b; see above). The surfaces  
221 are exposed in a small channel last occupied by meltwater during deglaciation, when  
222 water flowed north from three small lakes that currently drain towards the south-east  
223 (Figure 1c). The bedrock surface of the modern cliff at site 8 was used as the young control  
224 point with an age of zero years. This is justified on two grounds. First, this cliff surface was  
225 lichen free when the R-values were measured, which indicates a surface age of <25 years  
226 based on various estimates of the time required for the establishment of crustose *Rhizocarpon*  
227 lichens in Jotunheimen (Matthews, 2005; Matthews and Vater, 2015). Second, R-values from  
228 this cliff surface are similar but slightly higher than those characterising angular boulders

229 located about 100 m from the Vesle-Juvbreen glacier snout on terrain that, according to aerial  
230 photographic evidence, has an estimated age of 50 years (Matthews et al., 2014).

231

232 The resulting Schmidt-hammer exposure ages are derived with 95% confidence  
233 intervals ( $Ct$ ) that depend on the error associated with the calibration equation ( $Cc$ ) and  
234 the error of the surface to be dated ( $Cs$ ). This particular approach to SHD has been  
235 successfully applied to many different types of landforms composed of coarse rock  
236 particles and/or bedrock in southern Norway and elsewhere, including raised beaches  
237 (Shakesby et al., 2011), rock glaciers (Matthews et al., 2013), moraines (Matthews et  
238 al., 2014), pronival ramparts (Matthews and Wilson, 2015), snow-avalanche impact  
239 landforms (Matthews et al., 2015), periglacial patterned ground (Winkler et al., 2016),  
240 blockfields (Wilson and Matthews, 2016; Marr et al., 2018); blockstreams (Wilson et  
241 al., 2017) and rock-slope failures (Matthews et al., 2018b).

242

243 SHD was complemented by AMS radiocarbon dating of soil material within the  
244 regolith that overlies the bedrock beneath the terrace tread. The dated material  
245 constitutes a disturbed Humic Regosol (Ellis, 1979). Dating was carried out on bulk  
246 samples following acid wash pretreatment by Beta Analytic Inc using the INTCAL13  
247 database (Reimer et al., 2013) and Bayesian probability analysis (Bronk Ramsey,  
248 2009).

249

250 Organic content and particle size were measured for samples of soil and sub-  
251 soil. Weight loss-on-ignition at 550 °C (Heiri et al., 2001) was determined for samples  
252 dried at 105 °C. Particle size analysis involved sieving and further analysis of the <1  
253 mm fraction by laser diffraction using a Mastersizer 2000 (Malvern Instruments Ltd,

254 2007; Mingard et al., 2009).

255

256           Clast roundness and size, and the proportion of *in situ* fractured clasts, were  
257 measured on the terrace treads and cliffs as a basis for inferring the possible origins of  
258 clasts and the effectiveness of frost weathering processes. Clast roundness was assessed  
259 for boulders and cobbles comprising the surface of the inner and outer parts of the tread  
260 separately at each site using a five-point roundness scale (Powers, 1953) and a sample  
261 size of 150 clasts. Comparable samples of clasts resting on cliff ledges were also  
262 examined. The size (longest visible axis) of the largest 25 clasts was recorded separately  
263 for angular (roundness classes: very angular and angular) and edge-rounded clasts  
264 (roundness classes: subangular, subrounded and rounded) on the terrace treads. The  
265 proportion of fractured clasts on each terrace tread was determined, based on a sample  
266 size of 200 clasts.

267

268           Structural geological measurements made of the bedrock cliff included  
269 horizontal and vertical joint spacing ( $n = 25$ ): joints were defined as fractures or cracks  
270  $>1$  m long and  $>1$  mm wide. The strike and dip of metamorphic layering in the cliff face  
271 were also measured using a compass clinometer for comparison with layering in the  
272 buried bedrock terrace revealed by excavation of the regolith cover.

273

## 274 **RESULTS**

275

### 276 **Terrace morphology**

277

278 Morphology of the terraces is summarised by the cross-profiles from the 10 sites

279 (Figure 4) and illustrated further by general views of selected sites (Figure 5). All  
280 profiles have a similar northerly aspect. Terrace treads are 7.0 – 22.0 m wide and  
281 backing cliffs are 1.5 – 6.0 m high. Slope angles of the treads and cliffs are 2-12 ° and  
282 35-80 °, respectively, with a sharp break of slope or ‘knickpoint’ at the cliff base,  
283 sometimes resulting in an overhang (Figure 5c). No bedrock is visible at site 4, where a  
284 steep (30 °) boulder ‘ramp’ is assumed to bury a bedrock cliff. It should also be noted  
285 that the outer edge of the terraces at sites 5 and 6 terminate at low bedrock outcrops. At  
286 the other sites, the outer edge of the terrace tread is defined by a marked steepening of  
287 the slope. The height of the backing cliff is defined here conservatively as the relatively  
288 steep lowest part of the cliff, excluding the often degraded upper parts where there is a  
289 marked break of slope.

290

#### 291 **Clast characteristics on terrace treads and cliffs**

292

293 Clasts on the inner part of the terrace tread (Table 1) are invariably more angular  
294 (combined angular and very angular clasts, 14-77 %) than those on the outer part (5-35  
295 %). Furthermore, excluding site 4 (where the cliff is buried), the clasts on the cliffs are  
296 substantially more angular (49-97 %) than the clasts on the inner terrace treads.

297 Although there is no trend in roundness or size of clasts along the length of the main  
298 terrace, site 8 has consistently higher proportions of angular clasts than any of the other  
299 sites on both the inner and outer treads and on the backing cliff. Angular clasts  
300 predominate on cliffs at most sites but it is only at site 8 where the proportion  
301 approaches 100 %. Elsewhere, there is a variable mixture of angular and edge-rounded  
302 clasts, the proportion of angular clasts reaching only 13 % on the boulder ‘ramp’ at site  
303 4.

304

305           The size of the angular clasts on the treads tends to be larger (79-120 cm) than  
306 the size of the edge-rounded clasts (59-94 cm) with, in most cases, non-overlapping 95  
307 % confidence intervals. The proportion of *in situ* fractured clasts (Figure 6a) on the  
308 treads is consistently low at all sites (3.1-12.8 %) with < 6 % at most sites.

309

### 310 **Patterned ground on treads**

311

312 Sorted circles (Figure 6b) up to 2 m in diameter occasionally occur individually or in  
313 small groups in the low-angle tread surfaces. Their fine centres are clearly recognisable,  
314 but the outer boundaries of the clast-rich borders are poorly defined against the clast-  
315 covered tread surface. Poorly-defined solifluction lobes also occur in a few places on  
316 the treads. However, most tread surfaces are characterised by a thin cover of angular  
317 and edge-rounded clasts forming a largely undifferentiated pavement of boulders and  
318 cobbles. Where present, patches of fines are generally vegetated with mid-alpine grass-  
319 heath and snowbed plant communities.

320

### 321 **Subsurface bedrock, regolith and soil characteristics**

322

323 The underlying bedrock terrace was located beneath 60-80 cm of regolith at the  
324 excavation between sites 5 and 6 (Figure 7). The regolith consists of a matrix-  
325 supported diamicton, the <2 mm fraction of which consists of 43-83 % sand, 16-49 %  
326 silt and 2-8 % clay (n = 6 samples). Median grain-sizes of all six samples (50-150 µm)  
327 are frost susceptible according to textural limits for frost-susceptible sediments  
328 (Beskow, 1935; Harris, 1981).

329

330           A well-developed Humic Regosol (Ellis, 1979, 1980) has developed in the  
331 uppermost part of the regolith. This soil is up to 45-cm thick and characterised by  
332 disturbed organic-rich, dark grey-brown layers and streaks (organic content 13.1-15.2  
333 %) but no mineral horizon differentiation. With distance from the cliff base, the soil  
334 becomes lighter in colour and thinner and has more of the characteristics of an alpine  
335 Brown Soil (Ellis, 1979, 1980). Beneath the deepest organic-rich material, the lower  
336 part of the regolith (subsoil) has a much lower organic content (0.7-2.6 %), and an  
337 increasing density of rock fragments towards the underlying bedrock (see also Figure  
338 6c).

339

340           The bedrock terrace at the base of the excavation (Figure 7) has a slope of 3°,  
341 which is comparable to the slope of the terrace tread at the site (5°). That the bedrock  
342 terrace is indeed *in situ* is confirmed by the strike and dip of 167° (range 154–188°; n =  
343 3) and 22° NE (range 18–26°), which agree closely with the strike and dip in the  
344 exposed adjacent cliff of 138° (range 125–177°; n = 9) and 18° NE (range 10–26°). It  
345 should be noted that the second excavation failed to reach bedrock because of the  
346 presence of numerous large boulders throughout the regolith.

347

#### 348 **Joint spacing in cliffs**

349

350 Vertical and horizontal joints occur frequently in the cliffs, commonly with an increase  
351 in density near the cliff base (Figure 6d). The spacing of both vertical and horizontal  
352 joints is very variable, ranging from a few centimetres to 185 cm with no systematic  
353 pattern discernible between sites. Mean vertical and horizontal joint spacing (with 95 %

354 confidence intervals) for all sites is  $50 \pm 10$  and  $26 \pm 2$  cm, respectively; the closer  
355 spacing of horizontal joints reflecting the greater density of joints parallel to  
356 metamorphic layering, as seen in Figure 6d.

357

### 358 **Seepage water at the cliff/tread junction**

359

360 Water was observed seeping from joints at the base of the cliff at several sites despite  
361 former snowbeds having melted away earlier in the summer (Figure 8). The soil at the  
362 site of both excavations was damp, saturated with water in several places, and one of  
363 the trenches was slowly filling with water in late July 2018, despite the sites having  
364 experienced a severe drought for at least a month before these observations were made.  
365 Furthermore, a dry drainage channel crossed the tread of the terrace at site 2 beneath  
366 which the sound of flowing water could be heard, possibly indicative of piping.

367

### 368 **R-values from terrace treads and cliffs**

369

370 R-values for cliffs vary consistently along the length of the main terrace from a mean  
371 value of  $42.59 \pm 2.26$  at site 1 to  $59.66 \pm 1.24$  at site 8 (Table 2). The 95 % confidence  
372 intervals demonstrate, moreover, that this spatial variation along the main terrace is  
373 highly statistically significant. Cliff sites from the upper terraces (sites 9 and 10) exhibit  
374 intermediate values. The R-value distributions (Figure 9) consolidate these results and  
375 show highly variable, multimodal, negatively skewed and/or relatively broad platykurtic  
376 distributions indicative of mixed-age populations and hence diachronous surfaces  
377 (Matthews et al., 2014, 2015; Winkler et al., 2016; Marr et al., 2018). Only cliff site 8  
378 exhibits the low-variability, unimodal, symmetrical distribution of R-values that is



379 expected for a surface of uniform age. There is also a strong inverse relationship for  
380 cliff sites between R-value variability (as reflected in standard deviation values and  
381 confidence intervals) and mean R-values, which is consistent with an increase in  
382 variability as the extent of chemical weathering of the rock surfaces and the increase in  
383 mean rock surface age results in decreasing R-values (Aydin and Basu, 2005; Matthews  
384 et al, 2013, 2016).

385

386           Mean R-values from inner terrace treads at sites 2-8 are, in most cases,  
387 significantly lower than those from the corresponding cliffs by up to 7 units, and mean  
388 R-values from outer terrace treads tend to be even lower, though not significantly lower  
389 than those from the inner treads (Table 2). These patterns suggest that the mixed-age  
390 boulder populations on the inner terraces are older than those on the bedrock cliffs and  
391 that the boulder populations on the outer terraces are even older. Furthermore, the long  
392 tails that characterise most of the R-value distributions in Figure 9 are clearly the result  
393 of the relatively old component of mixed-age populations. Apart from site 1, all the  
394 outer tread sites have mean R-values within the relatively narrow range of 43.19-47.47  
395 and are therefore relatively old compared with the inner tread and cliff sites. Mean R-  
396 values from both the inner and outer treads at site 1 are, however, significantly higher  
397 than those of the corresponding cliff, which is not consistent with the results from the  
398 other sites and requires further explanation (see discussion below). At the upper terraces  
399 (sites 9 and 10), mean R-values from the terrace treads do not differ significantly from  
400 those of their cliffs and again exhibit intermediate values compared with the sites from  
401 the main terrace.

402

403 **Control point R-values and calibration equation**

404

405 R-values characterising potential control point surfaces from the local area (Table 3)  
406 include data from the mylonitised pyroxene-granulite gneiss surfaces used to derive the  
407 SHD calibration equation and calibration curve for this study (Figure 10). These data  
408 are close to but differ slightly from those relating to non-mylonitised pyroxene-granulite  
409 gneiss obtained in this study (G1 and G2 in Figure 1c and Table 3) and available from  
410 previous work (G3, from Matthews et al., 2014). Broad confidence intervals of the  
411 order of 1.0 R-value units reflect the variability of the local bedrock and suggest that R-  
412 values may be relatively high on recently exposed mylonite surfaces.

413

414         Although the ‘old’ control point derived from mylonite has yielded intermediate  
415 R-values with respect to non-mylonitised surfaces of the same known age, it  
416 nevertheless represents the best available for obtaining calibrated ages for the  
417 cryoplanation terraces. The fact that the mean R-value of the mylonitised ‘young’  
418 control-point surface exceeds that of non-mylonitised boulders recently exposed on the  
419 Vesl Juvbreen glacier foreland (Matthews et al., 2014) supports our use of the cliff  
420 surface as a modern control surface. Furthermore, the percentage frequency  
421 distributions of R-values for both control points (Figure 11) exhibit symmetrical  
422 distributions with no reason to doubt they are representative of single-age surfaces. It is  
423 particularly noteworthy that the distribution for the ‘old’ control point lacks the low R-  
424 values and negatively skewed distributions that are characteristic features of most of the  
425 terrace treads and cliffs.

426

427 **SHD ages**

428

429 The consistent decrease in SHD age of the cliffs along the length of the main terrace  
430 from  $8890 \pm 1185$  yr at site 1 to  $0 \pm 825$  yr at site 8 clearly shows spatial variation in  
431 exposure age from west to east (Table 4 and Figure 12). Indeed, there is a statistically  
432 significant linear relationship ( $r = 0.96$ ;  $p < 0.001$ ) between SHD age and distance from  
433 site 1 (Figure 13).

434

435 With the exception of site 1, confidence intervals show that the inner treads on  
436 the main terrace are consistently older than the cliffs, and there is a clear decrease in  
437 SHD age from sites 4 ( $7610 \pm 1210$  yr) through 8 ( $2605 \pm 1000$  yr), all of which have  
438 inner terraces that are significantly older than their cliffs. Although the linear  
439 relationship between SHD age and distance along the inner terrace is only marginally  
440 statistically significant when data from all eight sites are included ( $r = 0.65$ ;  $p < 0.10$ ;  
441 Figure 13), there is considerable improvement in the strength of this relationship ( $r =$   
442  $0.80$ ;  $p < 0.05$ ) if anomalous site 1 is omitted. The overlap in the confidence intervals for  
443 cliffs and inner treads at sites 2 and 3 indicate, however, little evidence of a significant  
444 difference in age. Also, again with the exception of site 1, the SHD ages of outer treads  
445 tend to be older than the inner treads but the age difference is relatively small and  
446 statistically significant only at sites 7 and 8 (Figure 12). Thus, in general, terrace treads  
447 are older than their corresponding cliffs, and outer treads are the oldest parts of the  
448 terraces, the SHD ages of which range from  $4690 \pm 1025$  yr at site 1 to  $8575 \pm 1270$  yr  
449 at site 4. However, there is little evidence of any systematic variation in SHD age within  
450 the outer treads.

451

452 The upper terraces exhibit little variation in SHD age between the two sites or  
453 between cliffs and treads. With all ages between  $5940 \pm 1040$  yr and  $7855 \pm 1130$  yr,

454 the exposure ages of the upper terraces are clearly intermediate between those of the  
455 youngest and oldest parts of the main terrace.

456

457 The anomalous pattern exhibited by site 1, where the cliff has a very much older  
458 exposure age than both the inner and outer treads (the SHD ages of which do not differ  
459 significantly from each other) is difficult to explain. Disturbance of the terrace tread by  
460 frost heave and frost sorting, bringing relatively unweathered boulders to the ground  
461 surface, provides a possible explanation.

462

### 463 <sup>14</sup>C ages

464

465 Two radiocarbon dates from two sides of the same trench, sampled at a distance of 50-  
466 60 cm from the cliff base, yielded a calibrated age between 3854 and 4821 cal yr BP at  
467 the 2σ range (Table 5 and Figure 7). This age estimate represents the maximum age of  
468 the overlying sedimentary material of the tread and a minimum age for the underlying  
469 bedrock platform at the sample point. The single date from the second excavation,  
470 sampled at a distance of 30 cm from the cliff, yielded the somewhat younger age  
471 estimate of 3345-3084 cal yr BP.

472

## 473 **DISCUSSION**

474

### 475 **Recognising cryoplanation terraces**

476

477 Cryoplanation terraces are problematic largely because their recognition and  
478 characterisation are based almost entirely on morphological evidence. There is a

479 tendency, moreover, to attribute all bench-like landforms on hillslopes in periglacial  
480 environments to cryoplanation (Ballantyne, 2018). Furthermore, most examples  
481 referred to in the literature appear to be relict and it has even been suggested that some  
482 such terraces are not characteristic of a periglacial environment at all, may be pre-  
483 Quaternary in age and/or may simply reflect geological structure (Büdel, 1982; French,  
484 2016, 2018). Although this study is heavily reliant on morphological evidence, an  
485 advantage of the cryoplanation terraces at Svartkampan is that they are currently active,  
486 at least in part. We are confident, therefore, that the combination of morphological  
487 evidence with dating evidence, field observations relevant to structure and process, and  
488 the general climatic characteristics of the sites, provides a firm basis for attributing their  
489 origin to cryoplanation.

490

#### 491 **Dating cryoplanation terraces**

492

493 There have been few previous attempts to date cryoplanation terraces, none of which  
494 has had much success. Vague generalisations have resulted from relative-age dating  
495 based on morphostratigraphy, weathering-rind thickness, vegetation or lichen cover  
496 (Péwé, 1970; Reger, 1975; Lauriol et al., 1997; Nelson, 1998). However, it has been  
497 concluded that they probably develop over very long periods of time, which supports  
498 similar ideas based on the observation that they are well developed in terrain that has  
499 never been glaciated or was not glaciated during the last glaciation (Reger and Péwé,  
500 1976; Lauriol and Godbout, 1988; Nelson and Nyland, 2017). To the authors'  
501 knowledge, the results of numerical-age dating techniques have been presented in two  
502 published papers only (Cremeens et al., 2005; Lauriol et al., 2006): the first applied  $^{36}\text{Cl}$   
503 cosmogenic-nuclide exposure-age dating to two possible cryoplanation summit flats;

504 the second obtained nine  $^{14}\text{C}$  dates from the regolith cover of the treads of undoubted  
505 cryoplanation terraces.

506

507 In the present study we have used two numerical-age dating techniques in the  
508 context of cryoplanation terraces for the first time, including the first application of  
509 SHD. Comparable results have been achieved from the extensive use of SHD on  
510 bedrock exposed in the backing cliffs and on the boulder cover of treads; and these  
511 results are in turn compatible with the  $^{14}\text{C}$  dating of organic sediments buried beneath  
512 the surface of treads. The SHD ages provide evidence of the extent to which the terraces  
513 are currently active, while the  $^{14}\text{C}$  ages provide estimates of maximum rates of cliff  
514 recession and terrace extension during the late Holocene. However, neither approach  
515 yields close estimates of landform age defined as the period of time over which the  
516 cryoplanation terraces formed.

517

#### 518 **SHD ages and current activity**

519

520 For a diachronous surface, SHD age estimates the average exposure-age of the sampled  
521 surface (Matthews et al., 2014, 2015; Winkler et al., 2016). The bedrock and boulder  
522 surfaces sampled from the cryoplanation terraces in this study vary considerably in their  
523 average exposure age (Table 4; Figure 12). Only the bedrock cliff sampled at site 8,  
524 with an SHD age of zero, is representative of a uniformly modern, active surface. All  
525 the other surfaces represent mixed-age populations, with increasing levels of activity  
526 and decreasing exposure-age and current activity along the length of the main terrace  
527 from west to east (sites 1 to 8). The remarkable linear SHD age and hence activity  
528 gradient exhibited by the cliffs (Figure 13) shows not only that the cliffs at the eastern

529 end of the main terrace are the most active but also that those at the western end are  
530 essentially relict. Indeed, the SHD age of the cliff at site 1 ( $8890 \pm 1185$  yr) indicates  
531 very little activity except <1000 yr after deglaciation.

532

533         The pattern of SHD ages between the cliffs, inner treads and outer treads, which  
534 is most apparent towards the eastern end of the main terrace (sites 5 to 8), is also  
535 enlightening (Figure 12). The fact that the inner tread is significantly older than the cliff  
536 at these sites, and that the outer tread is even older (significantly so at sites 7 and 8),  
537 points to the cliffs being the source of the relatively fresh boulders in the treads. These  
538 relatively fresh boulders, having been added to an older boulder population, would have  
539 reduced the average exposure-age of the surface boulders of the tread. This  
540 interpretation of the ages is supported by the clast roundness analyses, which  
541 demonstrate that the proportion of angular clasts in the cliffs is higher than on the treads  
542 and that the proportion on the inner treads tends to be higher than on the outer treads.  
543 Thus, the greater proportion of weathered clasts on the treads gives rise to the older  
544 SHD ages.

545

546         In theory, frost disturbance may reduce the exposure-age of clasts on the treads.  
547 Frost heave and frost sorting have the potential to bring relatively unweathered clasts to  
548 the surface, and frost fracturing of clasts embedded in the tread may expose fresh,  
549 unweathered rock surfaces. However, as the observed pattern of SHD ages (i.e. inner  
550 treads are older than cliffs and outer treads are characterised by the oldest ages) is the  
551 opposite of what would be the expected outcome of these disturbances, none of these  
552 disturbances are likely to have had an appreciable effect on the SHD ages (except,  
553 perhaps, at site 1).

554

555 **Rate of terrace formation and landform age**

556

557 The radiocarbon dates of ~3000, 4000 and 5000 cal yr BP for organic material at the  
558 base of the humic regosol at distances of 30, 50 and 60 cm, respectively, from the  
559 bedrock cliff (Table 5 and Figure 7) provide maximum estimates for the rate of bedrock  
560 cliff recession and terrace extension of ~0.10, 0.125 and 0.12 mm per year, respectively.  
561 These values are comparable to the measured rockwall recession rates compiled from a  
562 wide range of lithologies in arctic and alpine periglacial environments (Murton, 2013;  
563 Ballantyne, 2018; French, 2018).

564

565         Given that the deglaciation of Svartkampan occurred 9700 years ago, maximum  
566 cliff recession rates of the order of 0.1 mm per year are insufficient for the  
567 cryoplanation terraces to have been eroded entirely within the Holocene. Indeed,  
568 extrapolation of this rate implies that at least 56–176 ka would be required to erode the  
569 terraces, the widths of which range from 7–22 m. We conclude, therefore, that the onset  
570 of terrace formation is likely to have occurred prior to the last (Weichselian) glacial  
571 maximum, in periods with a periglacial climate. Subsequent survival of terraces also  
572 seems likely, which would have been possible under a relatively thin, cold-based ice  
573 sheet (cf. Kleman, 1994; Hättestrand and Stroeven, 2002; Juliussen and Humlum, 2007;  
574 Marr et al., 2018).

575

576         It must be acknowledged, however, that the inference of a wholly periglacial  
577 origin for the terraces depends on several assumptions, namely: (1) our estimated  
578 maximum rate of cliff recession is representative for the late Holocene; (2) similar rates



579 can be applied to the entire Holocene and also to pre-Holocene periglacial regimes; and  
580 (3) alternative processes (such as differential subglacial erosion) did not contribute to  
581 these landforms. The third assumption may not be reasonable, given the nature of the  
582 regolith that covers the bedrock surface of the treads. It is apparent that much of the  
583 regolith consists of a diamicton, with numerous edge-rounded clasts and abundant fine  
584 matrix. Similar edge-rounded clasts occur on the cliffs and completely bury the cliff at  
585 site 4. Both the diamicton and the edge-rounded clasts most likely originated as till,  
586 deposited during deglaciation and subsequently reworked by periglacial mass wasting.  
587 It is not unrealistic to suggest, therefore, that subglacial erosion through plucking  
588 contributed to preparation and erosion of the cliff prior to the Holocene and hence could  
589 account for a substantial share of the present-day width of the terraces.

590

#### 591 **Frost-weathering processes on the cliffs**

592

593 Frost weathering is conventionally regarded as the primary process in explaining the  
594 backwearing of cliffs in the context of cryoplanation terraces (Boch and Krasnov, 1943,  
595 Demek, 1969a; 1969b; Priesnitz, 1988; Czudek, 1995). However, the sparsity of direct  
596 process studies has been universally recognised as a major problem in their  
597 interpretation. Nevertheless, several lines of indirect evidence from Svartkampan point  
598 strongly to the main process being the production of relatively large rock fragments by  
599 frost wedging (alternatively termed macrogelivation) as a result of the freezing of water  
600 in pre-existing cracks) (Murton, 2013; Ballantyne, 2018).

601

602 First, the modern cliff at site 8 and active parts of cliffs at the other sites are  
603 clearly the main source of the clasts littering the inner treads of the terraces. These well-

604 jointed cliffs (frost-riven cliffs to use the term commonly employed in cryoplanation  
605 research) produce clasts that match those on the inner treads in terms of exposure-age,  
606 angularity and size. The low proportions of *in situ* fractured clasts on the treads  
607 indicates, moreover, that comminution of existing clasts is not a feasible alternative  
608 source for abundant, large angular clasts on the treads (cf. Berrisford, 1991).

609

610         Second, abundant moisture is available at the base of the cliffs from  
611 groundwater, which originates from permafrost thaw and summer rainfall as well as  
612 snowmelt. Water is as essential as sub-zero temperatures for frost weathering (Hall et  
613 al., 2002; Thorn and Hall, 2002; Thorn et al., 2011). It remains available at the  
614 Svartkampan sites during freeze-back, enabling ice to form in pre-existing joints and  
615 cracks. Frost wedging is most likely to occur at this time in response not only to the  
616 volumetric expansion of ice in the cracks but also to the growth of segregation ice as  
617 water migrates towards a freezing front that is penetrating deep into the cliff (cf. Walder  
618 and Hallet, 1985; Matthews et al., 1986; Hallet et al., 1991; Murton et al., 2006;  
619 Matsuoka and Murton, 2008). Although the development of segregation ice has been  
620 investigated and discussed largely in relation to porous rocks, it would also be expected  
621 in association with interconnected microcracks in the layered mylonitised gneiss at  
622 Svartkampan. Significantly, cryoplanation terraces and other frost-riven cliffs in the  
623 Sudetes Mountains (Central Europe) appear to be preferentially associated with gneissic  
624 and schistose bedrock (Traczyk and Migon, 2000).

625

626         Third, evidence for fractured bedrock and *in situ*, loosely-attached rock  
627 fragments forming breccia, is particularly abundant close to the foot of the cliff, both  
628 above (Figure 6d) and below (Figure 6c) the surface of the tread. This is precisely

629 where groundwater seepage occurs, and hence where most water is available for ice  
630 formation in cracks, and where frost weathering would be expected to undercut the cliff,  
631 producing the sharp cliff/tread junction and maintaining the terrace cross-profile shape.  
632 Maximum seepage at the cliff base is attributed to the topography of the ground surface,  
633 combined with high joint density and the configuration of the still-frozen substrate.

634

635 Fourth, both cliff and buried bedrock surfaces (Figure 7) cut across bedrock  
636 structures, effectively excluding an explanation based purely on geology. In the absence  
637 of evidence for alternative processes capable of producing flights of such terraces, this  
638 has generally been accepted as strong evidence for cliff recession as a result of frost  
639 weathering, provided debris removal by mass wasting is sufficient to prevent the  
640 accumulation of debris at the cliff base (Demek, 1969a, Presnitz, 1988; Czudek, 1995;  
641 Nelson and Nyland, 2017).

642

#### 643 **Transport processes on the treads**

644

645 Transport of sediments across the treads of cryoplanation terraces is commonly  
646 attributed to solifluction and flowing water, with gelifluction, frost creep, slopewash,  
647 sheet wash, snow meltwater, suprapermafrost meltwater, infiltration water, subsurface  
648 flow, piping, and suffosion, all having been mentioned in the literature (Demek, 1969a;  
649 Czudek and Demek, 1971; Reger and Péwé, 1975; Presnitz, 1988; Lauriol, 1990;  
650 Czudek, 1995). Solifluction and various types of water flow occur at Svartkampan, but  
651 the observational and dating evidence presented above indicate that such transport must  
652 have been extremely slow throughout the Holocene. Although supranival transport  
653 cannot be ruled out as a contributory process, the coarser material could not have been

654 moved by most of the water-flow processes. Furthermore, many of the edge-rounded  
655 surface clasts and most of the silty-sand matrix comprising the regolith seem to have  
656 originated as till, which was deposited during deglaciation. Subsequently, the frost-  
657 susceptible regolith was disturbed by solifluction but, according to our dating, it was  
658 transported no more than a few metres across the terraces during the Holocene.

659

660 Solution (Rapp, 1960; Lauriol et al., 1997; Thorn et al., 2011) and wind  
661 transport (Demek, 1969a; Lauriol et al., 1997; Lamirande et al., 1999) probably  
662 contributed to the removal of some fines from the regolith at some places and times, but  
663 these processes cannot have had a major effect on the overall volume and fabric of the  
664 regolith over the Holocene timescale. Similarly, cryoturbation and frost sorting  
665 undoubtedly contributed to disturbance of the frost-susceptible regolith, and may well  
666 have favoured infiltration, the concentration of surface and subsurface water flow and  
667 piping (Presnitz, 1988) while leaving the bulk of the regolith intact.

668

#### 669 **Developmental model of cryoplanation terraces**

670

671 Various seasonal processes contribute to the development of active cryoplanation  
672 terraces at Svartkampan. The presence of groundwater near the cliff base during autumn  
673 and early winter freeze-back is of critical importance (Figure 14a). At this time,  
674 groundwater is moving downslope under gravity along cracks and joints within the  
675 active layer of the cliff and emerging near the base of the cliff where the groundwater  
676 table intersects the ground surface. Permafrost and/or infiltration of rainwater must be  
677 the major water source as, by this time, the late-lying snowbeds have melted away.  
678 Also, groundwater in the active layer cannot penetrate the permafrost, which is acting as

679 an aquiclude, or at least an aquitard (Woo, 2012; Liao and Zhuang, 2017). Thus, above  
680 the permafrost table, and especially at the cliff base, groundwater is available for ice  
681 wedging and/or the growth of segregation ice during refreezing of the active layer.

682

683         Transportation of debris across the terrace tread takes place mainly during the  
684 spring and early summer, when thaw consolidation leads to solifluction and snow  
685 meltwater is abundant (Figure 14b). Also in spring and summer, melting of ice in the  
686 cliff is likely to trigger rockfall onto the terrace tread, either directly or indirectly via the  
687 snowbed surviving at that time on the inner tread. However, rates of solifluction are  
688 very slow due to the low gradient of the tread and the outer tread tends to be more stable  
689 than the inner tread, affected less by solifluction and perhaps more by cryoturbation and  
690 frost sorting. Beneath the regolith-covered inner terrace tread, the active layer is likely  
691 to be thinner than beneath the bedrock cliff, because of its higher ice content and  
692 consequent greater amount of latent heat required to thaw the ground. In addition, the  
693 active layer will tend to be thinner under the snowbed due to the insulating properties of  
694 late-lying snow. Conditions are different on the tread during freeze-back: the snowbed  
695 has melted away, surface sediments are drier, and the reduced availability of water leads  
696 to relatively low rates of bedrock frost weathering beneath the tread.

697

698         Over the long-term, the zone of maximum frost weathering close to the cliff  
699 base leads to the cliff being undercut, and to parallel retreat of a near-vertical cliff  
700 (Figure 14c). This model bears some similarity to that originally proposed by Boch and  
701 Krasnov (1943), namely enhanced frost weathering towards the cliff base,  
702 comparatively little lowering of the bedrock beneath the terrace tread, parallel retreat of  
703 the cliff over time, and solifluction as the main process evacuating sediment across the

704 tread. However, several important new features of our model should be highlighted,  
705 particularly: (1) *undercutting* of the cliff by frost weathering at the cliff-tread junction,  
706 which produces and maintains a *near-vertical* cliff; (2) provision of a *groundwater-*  
707 *based mechanism* for cliff recession; (3) *seasonal dimensions* to both cliff recession and  
708 sediment evacuation from the tread; and (4) *negligible* lowering over time of the near-  
709 horizontal bedrock surface beneath the tread, attributed to the thermal properties of the  
710 regolith cover, leading to a relatively thin active layer, which may not penetrate far into  
711 the bedrock.

712

### 713 **Structural control of terrace initiation?**

714

715 As with earlier models that more-or-less require an initial cliff-like form, our model  
716 does not provide an explanation for the initiation of cryoplanation terrace  
717 development. Without an appropriate pre-existing landform, it is difficult to see how  
718 enhanced frost-weathering would produce such a cliff on a land surface with a  
719 uniform slope angle. Possible precursors (proto-cliffs) might be controlled by  
720 geological structure and/or accentuated by selective glacial erosion at times when a  
721 Pleistocene ice-sheet was not cold-based and protective. Dilatation joints and  
722 exfoliation following repeated glacial loading and unloading might also be considered  
723 but, ultimately, no definite answer can be given. From their alignment and location, at  
724 least some form of structural control of a proto-cliff seems likely (though subsequent  
725 cliff retreat does not follow the smaller-scale bedrock structures).

726

### 727 **Permafrost promotes cryoplanation**

728

729 Reger and Péwé (1976) argued strongly that cryoplanation requires permafrost, and it  
730 seems to be accepted that the most favourable conditions occur where permafrost is  
731 present under relatively continental climates (Crudek, 1995; Hall, 1998; Nelson and  
732 Nyland, 2017). Our research at Svartkampan indicates that permafrost is an important  
733 water source for frost weathering and solifluction, and that an impermeable permafrost  
734 table confines meltwater flow to the active layer, contributes to the focusing of frost  
735 weathering towards the cliff base, and provides a ‘base level’ below which frost  
736 weathering is ineffective. Apparently active cryoplanation terraces have nevertheless  
737 been described from areas with deep seasonal ground freezing, such as low-alpine zones  
738 and maritime polar regions (Demek 1969a; Schunke and Heckendorff, 1976; Crudek  
739 1995). In view of slow rates of development, however, it is difficult to establish whether  
740 such terraces experienced seasonal freezing throughout their development. Thus, we  
741 conclude that although permafrost promotes cryoplanation it cannot yet be said to be a  
742 necessary condition.

743

#### 744 **Cryoplanation is not the same as nivation**

745

746 It has been suggested that there are similarities in the morphology and genesis of  
747 cryoplanation terraces and nivation benches or hollows (Margold et al., 2011;  
748 Ballantyne, 2018), and that cryoplanation and nivation can be conceptualised as  
749 representing different parts of a single process spectrum (Hall, 1998; Thorn and Hall,  
750 2002). An important insight following from our research on the Svartkampan terraces,  
751 however, is that snow, and processes of nivation, play only a secondary role in  
752 cryoplanation and the formation of cryoplanation terraces. This is in agreement with  
753 the proposal of Hall (1998) and Thorn and Hall (2002) that cryoplanation is associated

754 with relatively cold climates, permafrost and snow-free conditions, whereas nivation  
755 is characterised by the presence of snow in milder and wetter climates. Thus, we  
756 propose that cryoplanation should be regarded as essentially distinct from nivation.

757

758         The characteristic process of cryoplanation and our model of cryoplanation  
759 terrace development is frost weathering at the cliff base: this leads, over time, to the  
760 parallel retreat of the cliff and terrace extension (Figure 14c). Thermal insulation by  
761 snow dampens the annual freeze-thaw cycle rather than accentuates it (Draebing et al.,  
762 2017) and, most importantly, snow is normally no longer available as a moisture source  
763 during freeze-back. Water for ice-growth at this time comes from groundwater – supra-  
764 permafrost meltwater flow and infiltration water from autumn rainfall – rather than  
765 snowbeds. Thus, any late snowbeds on the terrace treads (see, for example Figure 2) are  
766 an effect rather than a cause of the cryoplanation terrace and, more likely than not, slow  
767 down the rate of cliff recession and terrace extension. Interestingly, the original  
768 definition of nivation (Matthes, 1900) did not include frost weathering of bedrock.

769

770         Processes of nivation (snow-generated processes capable of enhancing  
771 geomorphic work) (cf. Thorn, 1976, 1988; Thorn and Hall, 1980, 2002; Nyberg, 1991;  
772 Christiansen, 1998a, 1998b) do contribute to the transport of material across the terrace  
773 tread. During spring and summer thaw, solifluction occurs beneath and in front of  
774 snowbeds on the tread, and snow meltwater transports fine sediments away from the  
775 cliff while rockfall material from the cliff may undergo supranival transport (Figure  
776 14a). However, the dates obtained on both organic sediments and surface boulders in  
777 this study demonstrate extremely slow Holocene transport rates with relatively small  
778 quantities of material being transported for a short distance across the inner terrace



779 tread, which leaves the outer tread in an essentially relict state.

780

## 781 **SUMMARY AND CONCLUSIONS**

782

783 We have dated cryoplanation terraces for the first time using two different dating  
784 techniques and present a process-based conceptual model of cryoplanation terrace  
785 development. SHD was applied to surface boulders on terrace treads and bedrock cliffs  
786 and  $^{14}\text{C}$  dating was applied to organic-rich sediment within the regolith on the tread.  
787 This chronological information, combined with observational evidence, has enabled  
788 several controversial aspects of cryoplanation to be addressed.

789

790         The statistically significant decrease in SHD mean age ( $\pm 95\%$  confidence  
791 interval) of the cliffs along the length of the main terrace, from  $8890 \pm 1185$  yr at site 1  
792 to  $0 \pm 825$  yr at site 8, demonstrates significant spatial variation in exposure age and  
793 activity. This strong west-east age gradient seems to reflect subtle topographic  
794 variations with consequent effects on groundwater hydrology and frost weathering.  
795 With the exception of site 1, the inner treads on the main terrace yielded consistently  
796 older SHD ages than the cliffs, and the SHD ages of outer treads tend to be older than  
797 the inner treads. None of the SHD ages are older than the Holocene but most terraces  
798 have active and relict elements. The SHD ages are complemented by three  $^{14}\text{C}$  dates of  
799 between 3854 and 4821 cal yr BP ( $2\sigma$  range), which indicate a maximum rate of cliff  
800 recession of the order of 0.1 mm per year. Extrapolation of this rate suggests that the  
801 terraces began to form before the last glacial maximum, survived glaciation beneath  
802 cold-based ice, and resumed active development in the Holocene.

803

804           Excavation has demonstrated that the terraces cut across bedrock structures yet  
805 most of the regolith on the terrace treads is interpreted as diamicton derived from till  
806 deposited during deglaciation and subsequently reworked by solifluction and  
807 cryoturbation. Boulder pavement caps much of the regolith on the inner treads and the  
808 pavement tends to be formed of angular boulders derived from the cliffs; whereas on  
809 the outer treads, edge-rounded clasts are characteristic. The age, angularity and size of  
810 clasts on the inner treads supports frost-weathering as the primary process leading to  
811 cliff recession and terrace extension. During autumn freeze-back, snowbeds have  
812 melted yet seepage water is still available at the cliff-base, where effective frost  
813 wedging and/or the growth of segregation ice in joints and cracks is inferred to occur  
814 during prolonged winter frost penetration. Thus, the availability of groundwater during  
815 freeze-back is considered to be critical for cryoplanation, which proceeds slowly by  
816 parallel retreat of a cliff undercut by frost weathering.

817

818           Permafrost seems to promote the formation of well-developed cryoplanation  
819 terraces by providing an impermeable frost table beneath the active layer, focusing  
820 groundwater flow towards the cliff base, and supplying water during spring and  
821 summer thaw. Together with snowmelt, supra-permafrost meltwater promotes the  
822 transport of regolith across the terrace surface, especially by solifluction following thaw  
823 consolidation. However, such transport processes are very slow under the relatively  
824 continental climatic conditions of northeastern Jotunheimen. It is argued that seasonal  
825 frost is less likely to promote cryoplanation and terrace development.

826

827           Contrary to the view expressed in several recent publications, our results  
828 suggest that cryoplanation should be seen as different from nivation. Snow appears to

829 play, at most, only a secondary role in cryoplanation. And enhanced frost weathering  
830 linked to groundwater hydrology during freeze-back, which is so important for  
831 cryoplanation, does not constitute a nivational process.

832

### 833 **ACKNOWLEDGEMENTS**

834

835 Fieldwork was carried out on the Swansea University Jotunheimen Research  
836 Expeditions, 2017 and 2018. We thank Anika Donner for assistance in the field, Charles  
837 Harris for discussions on the possible effects of permafrost, named (Martin Margold  
838 and Atle Nesje) and unnamed reviewers for comments leading to improvement of the  
839 manuscript, Ole Jakob and Tove Grindvold for logistical support, and Anna Ratcliffe  
840 for drawing up the figures for publication. This paper constitutes Jotunheimen Research  
841 Expeditions Contribution No. 207 (see: <http://jotunheimenresearch.wixsite.com/home>)

842

### 843 **REFERENCES**

844

845 Aydin, A., Basu, A., 2005. The Schmidt hammer in rock material characterisation.  
846 *Engineering Geology* 81, 1-14.

847

848 Ballantyne, C.K., 2018. *Periglacial Geomorphology*. Wiley-Blackwell: Chichester.

849

850 Barnett, C., Dumayne-Peaty, L., Matthews, J. A., 2000. Holocene climatic change and  
851 tree-line response in Leirdalen, central Jotunheimen. *Review of Palaeobotany and*  
852 *Palynology* 117, 119–137.

853

854 Berrisford, M.S., 1991. Evidence for enhanced mechanical weathering associated with  
855 seasonally late-lying and perennial snow patches, Jotunheimen, Norway. *Permafrost*  
856 *and Periglacial Processes* 2, 331-340.

857

858 Beskow, G., 1935. Tjälbildningen och tjällyftningen med särskild hänsyn till vägar och  
859 järnågar. Sveriges *Geologiske Undersökning, Series C 375, Årbok 26*, 1-242.  
860

861 Boch, S.G., Krasnov, I.I., 1943. On altiplanation terraces and ancient surfaces of  
862 levelling in the Urals and associated problems. In: Evans, D.J.A. (Ed.), (1994) *Cold*  
863 *Climate Landforms*. Wiley, Chichester, pp. 177-186. [Translated from Russian]  
864

865 Bronk Ramsey, C., 2009. Bayesian analysis of radiocarbon dates. *Radiocarbon* 51, 337-  
866 360.  
867

868 Büdel, J. 1981. *Klima- Geomorphologie, 2nd edition*. Bornträger, Berlin-Stuttgart.  
869

870 Christiansen, H.H., 1998a. Nivation forms and processes in unconsolidated sediments,  
871 NE Greenland. *Earth Surface Processes and Landforms* 23, 751-760.  
872

873 Christiansen, H.H., 1998b. 'Little Ice Age' nivation activity in northeast Greenland. *The*  
874 *Holocene* 8, 719-728.  
875

876 Cremeens, D.L., Darmody, R.G., George, S.E., 2005. Upper slope landforms and age of  
877 bedrock exposures in the St. Francois Mountains, Missouri: a comparison of relict  
878 periglacial features in the Appalachian Plateau of West Virginia. *Geomorphology* 70,  
879 71-84.  
880

881 Czudek, T., 1995. Cryoplanation terraces – a brief review and some remarks.  
882 *Geografiska Annaler Series A (Physical Geography)* 77A, 95-105.  
883

884 Czudek, T., Demek, J., 1971. Pleistocene cryoplanation in the Česká Vpocina  
885 highlands, Czechoslovakia. *Transactions of the Institute of British Geographers* 52, 95-  
886 112.  
887

888 Dahl, S.O., Nesje, A., Lie, Ø., Fordheim, K., Matthews, J.A., 2002. Timing,  
889 equilibrium-line altitudes and climatic implications of two early-Holocene readvances  
890 during the Erdalen Event at Jostedalsbreen, western Norway. *The Holocene* 12, 17-25.  
891

892 Demek, J., 1968. Cryoplanation terraces in Yakutia. *Biuletyn Peryglacjalny* 17, 91-116.  
893

894 Demek J., 1969a. Cryoplanation terraces, their geographical distribution, genesis and  
895 development. *Rozprawy Československé Akademie Věd, Rada Matematických a*  
896 *Prírodních Věd Rocnik* 79(4): 80pp.  
897

898 Demek, J., 1969b. Cryogene processes and the development of cryoplanation terraces.  
899 *Biuletyn Peryglacjalny* 18, 115-125.  
900

901 Draebing, D., Haberkorn, A., Krautblatter, M., Kenner, R., Phillips, M. 2017. Thermal  
902 and mechanical responses resulting from spatial and temporal snow cover variability in  
903 permafrost rock slopes, Steintaelli, Swiss Alps. *Permafrost and Periglacial Processes*  
904 28, 140-157.  
905

906 Ellis, S., 1979. The identification of some Norwegian mountain soil types. *Norsk*  
907 *Geografisk Tidsskrift* 33, 205-212.  
908

909 Ellis, S., 1980. Soil-environmental relationships in the Okstindan Mountains, north  
910 Norway. *Norsk Geografisk Tidsskrift* 34, 167-176.  
911

912 Farbrot, H., Hipp, T.F., Etzelmüller, B., Isaksen, K., Ødegård, R.S., Schuler, T.V.,  
913 Humlum, O., 2011. Air and ground temperature variations observed along elevation  
914 and continentality gradients in southern Norway. *Permafrost and Periglacial*  
915 *Processes* 22, 343–360.  
916

917 French, H.M., 2016. Do periglacial landforms exist? A discussion of the upland  
918 landscapes of northern interior Yukon, Canada. *Permafrost and Periglacial Processes*  
919 27, 219-228.  
920

921 French, H.M., 2018. *The Periglacial Environment*, 4<sup>th</sup> edition. Wiley-Blackwell:  
922 Chichester.  
923

924 Goehring, B. M., Brook, E. J., Linge, H., Raisbeck, G. M., Yiou, F., 2008. Beryllium-  
925 10 exposure ages of erratic boulders in southern Norway and implications for the  
926 history of the Fennoscandian Ice Sheet. *Quaternary Science Reviews* 27, 320–336.  
927

928 Grosso, S.A., Corte, A.E., 1991. Cryoplanation surfaces in the Central Andes at latitude  
929 35° S. *Permafrost and Periglacial Processes* 2, 49-58.  
930

931 Hall, K., 1997. Observations on “cryoplanation” benches in Antarctica. *Antarctic*  
932 *Science* 9, 181-187.  
933

934 Hall, K., 1998. Nivation or cryoplanation: different terms, same features? *Polar*  
935 *Geography* 22, 1-16.  
936

937 Hall, K., André, M.-F., 2010. Some further observations regarding “cryoplanation  
938 terraces” on Alexander Island. *Antarctic Science* 22, 175-183.  
939

940 Hall, K., Thorn, C.E., Matsuoka, N., Prick, A., 2002. Weathering in cold regions: some  
941 thoughts and perspectives. *Progress in Physical Geography* 26, 577-603.  
942

943 Hallet, B., Walder, J.S., Stubbs, C.W., 1991. Weathering by segregation ice growth in  
944 microcracks at sustained sub-zero temperatures: verification from an experimental  
945 study using acoustic emission. *Permafrost and Periglacial Processes* 2, 283-300.  
946

947 Harris, C., 1981. *Periglacial Mass Wasting: a Review of Research*. Geobooks, Norwich  
948 [British Geomorphological Research Group Research Monograph 4].  
949

950 Harris, C., Arenson, L.U., Christiansen, H.H., Etzelmüller, B., Frauenfelder, R.,  
951 Gruber, S., Haeberli, W., Hauck, C., Hoelzle, M., Humlum, O., Isaksen, K., Käab, A.,  
952 Kern-Luetschg, M.A., Lehning, M., Matsuoka, N., Murton, J.B., Noezli, J., Phillips,  
953 M., Ross, N., Seppälä, M., Springman, S.M., Vonder Mühll, D.V., 2009. Permafrost  
954 and climate in Europe: monitoring and modelling thermal, geomorphological and  
955 geotechnical responses. *Earth Science Reviews* 92, 117–171.  
956

957 Harris, S.A., Brouchkov, A., Cheng G., 2018. *Geocryology: Characteristics and Use of*

958 *Frozen Ground and Periglacial Landforms*. CRC Press-Balkema: Leiden.  
959  
960 Hättestrand, C., Stroeven, A.P., 2002. A relict landscape in the centre of the  
961 Fennoscandian glaciation: geomorphological evidence of minimal Quaternary glacial  
962 erosion. *Geomorphology* 44, 127-143.  
963  
964 Heiri, O., Lotter, A.F., Lemcke, G., 2001. Loss on ignition as a method for estimating  
965 organic and carbonate content in sediments: reproducibility and comparability of  
966 results. *Journal of Paleolimnology* 25, 101-110.  
967  
968 Hipp, T., Etzelmüller, B., Westermann, S., 2014. Permafrost in alpine rock faces from  
969 Jotunheimen and Hurrungane, southern Norway. *Permafrost and Periglacial*  
970 *Processes* 25, 1–13.  
971  
972 Hormes, A., Blaauw, M., Dahl, S.-O., Nesje, A., Possnert, G., 2009. Radiocarbon  
973 wiggle-match dating of proglacial lake sediments – implications for the 8.2 ka event.  
974 *Quaternary Geochronology* 4, 267–277.  
975  
976 Hughes, A. L. C., Gyllencreutz, R., Lohne, Ø., Mangerud, J., Svendsen, J. L., 2016.  
977 The last Eurasian ice sheets – a chronological database and time-slice reconstruction,  
978 DATED-1. *Boreas* 45, 1–45.  
979  
980 Isaksen, K., Hauck, C., Gudevang, E., Ødegård, R.S., Sollid, J.L., 2002. Mountain  
981 permafrost distribution in Dovrefjell and Jotunheimen, southern Norway, based on  
982 BTS and DC resistivity tomography data. *Norsk Geografisk Tidsskrift* 56, 122–136.  
983  
984 Isaksen, K., Ødegård, R.S., Etzelmüller, B., Hilbich, C., Hauck, C., Farbot, H.,  
985 Eiken, T., Hagen, J.O., Hipp, T.F., 2011. Degraded mountain permafrost in southern  
986 Norway: spatial and temporal variability of ground temperatures, 1999–2009.  
987 *Permafrost and Periglacial Processes* 22, 361–377.  
988  
989 Juliussen, H., Humlum, O., 2007. Preservation of blockfields beneath Pleistocene ice  
990 sheets on Solen and Elgahogna, central-eastern Norway. *Zeitschrift für*  
991 *Geomorphologie N.F.* 51, Supplementband 2, 113-138.

992  
993 Kleman, J., 1994. Preservation of landforms under ice sheets and ice caps.  
994 *Geomorphology* 9, 19-32.  
995  
996 Křížek, M., 2007. Periglacial landforms above the alpine timberline in the High  
997 Sudetes. In Goudie, A.S and Kalvoda, J. (eds) *Geomorphological Variations*, 313-337.  
998 P3K Publishing, Prague.  
999  
1000 Lamirande, I., Lauriol, B., Lalonde, A.E., Clark, I.D., 1999. La production de limon sur  
1001 tes terrasses de cryoplanation dans les Monts Richardson, Canada. *Canadian Journal of*  
1002 *Earth Sciences* 36, 1645-1654. et al., 1999  
1003  
1004 Lauriol, B., 1990. Cryoplanation terraces, northern Yukon. *Canadian Geographer* 34,  
1005 347-351.  
1006  
1007 Lauriol, B., Godbout, L., 1988. Les terrasses de cryoplanation dans le nord du Yukon:  
1008 distribution, genèse et âge. *Geographie Physique et Quaternaire* 42, 303-314.  
1009  
1010 Lauriol, B.M., Lalonde, A.E., Dewez, V., 1997. Weathering of quartzite on a  
1011 cryoplanation terrace in northern Yukon. *Permafrost and Periglacial Processes* 8, 147-  
1012 153.  
1013  
1014 Lauriol, B., Lamirande, I., Lalonde, A.E., 2006. The Giant Steps of Bug Creek,  
1015 Richardson Mountains, N.W.T., Canada. *Permafrost and Periglacial Processes* 17,  
1016 267-275.  
1017  
1018 Liao, C., Zuang, Z., 2017. Quantifying the role of permafrost distribution in  
1019 groundwater and surface water interactions using a three-dimensional hydrological  
1020 model. *Arctic, Antarctic and Alpine Research* 49, 81-100.  
1021  
1022 Lilleøren, K.S., Etzelmüller, B., Schuler, T.V., Ginås, K., Humlum, O., 2012. The  
1023 relative age of permafrost – estimation of Holocene permafrost limits in Norway.  
1024 *Global and Planetary Change* 92–93, 209–223.  
1025



1026 Lutro, O., Tveten, E., 1996. *Geologiske kart over Norge, bergrunnskart Årdal,*  
1027 *1:250,000.* Norges Geologiske Undersøkelse, Trondheim.

1028

1029 Malvern Instruments Ltd., 2007. *Mastersizer 2000, User Manual. MAN0384, Issue 1.0.*  
1030

1031 Mangerud, J., Gyllencreutz, R., Lohne, Ø., Svendsen, J.I., 2011. Glacial history of  
1032 Norway. In: Ehlers, J., Gibbard, P.L., Hughes, P.D. (Eds.), *Quaternary Glaciations –*  
1033 *Extent and Chronology: a Closer Look.* Elsevier, Amsterdam, pp. 279-298.

1034

1035 Margold, M., Treml, V., Petr, L., Nyplová, P., 2011. Snowpatch hollows and pronival  
1036 ramparts in the Krkonose Mountains, Czech Republic: distribution, morphology and  
1037 chronology of formation. *Geografiska Annaler Series A (Physical Geography)* 93A,  
1038 137-150.

1039

1040 Marr, P., Winkler, S., Löffler, J., 2018. Investigations on blockfields and related  
1041 landforms at Blåhø (Southern Norway) using Schmidt hammer exposure-age dating:  
1042 palaeoclimatic and morphodynamic implications. *Geografiska Annaler Series A*  
1043 *(Physical Geography)* 100A, 285-306.

1044

1045 Matthes, F.E., 1900. Glacial sculpture of the Bighorn Mountains, Wyoming. *United*  
1046 *States Geological Survey 21<sup>st</sup> Annual Report 1899-1900*, 167-190.

1047

1048 Matthews, J.A., 2005. ‘Little Ice Age’ glacier variations in Jotunheimen, southern  
1049 Norway.: a study in regionally-controlled lichenometric dating of recessional moraines  
1050 with implications for climate and lichen growth rates. *The Holocene* 15, 1-19.

1051

1052 Matthews, J. A., McEwen, L. J., 2013. High-precision Schmidt hammer exposure-age  
1053 dating (SHD) of flood berms, Vetlestølsdalen, alpine southern Norway: first  
1054 application and some methodological issues. *Geografiska Annaler Series A, Physical*  
1055 *Geography* 95, 185–194.

1056

1057 Matthews, J. A., Owen, G., 2010. Schmidt-hammer exposure-age dating: developing  
1058 linear age-calibration curves using Holocene bedrock surfaces from the Jotunheimen-  
1059 Jostedalbreen regions of southern Norway. *Boreas* 39, 105–115.

1060

1061 Matthews, J.A. and Vater, A.E., 2015. Pioneer zone geo-ecological change:  
1062 observations from a chronosequence on the Storbreen glacier foreland, Jotunheimen,  
1063 southern Norway. *Catena* 135, 219-230.

1064

1065 Matthews, J. A., Wilson, P., 2015. Improved Schmidt-hammer exposure ages for  
1066 active and relict pronival ramparts in southern Norway, and their palaeoenvironmental  
1067 implications. *Geomorphology* 246, 7–21.

1068

1069 Matthews, J. A., Winkler, S., 2011. Schmidt-hammer exposure-age dating (SHD):  
1070 application to early Holocene moraines and a reappraisal of the reliability of terrestrial  
1071 cosmogenic-nuclide dating (TCND) at Austanbotnbreen, Jotunheimen, Norway.  
1072 *Boreas* 40, 256–270.

1073

1074 Matthews, J.A., Dawson, A.G., Shakesby, R.A., 1986. Lake shoreline development,  
1075 frost weathering and rock platform erosion in an alpine periglacial environment,  
1076 Jotunheimen, southern Norway. *Boreas* 15, 33-50.

1077

1078 Matthews, J. A., Berrisford, M.S., Dresser, P.Q., Nesje, A., Dahl, S.-O., Bjune, A. E.,  
1079 Bakke, J., Birks, H. J. B., Lie, Ø., Dumayne-Peaty, L., Barnett, C., 2005. Holocene  
1080 glacier history of Bjørnbreen and climatic reconstruction in central Jotunheimen,  
1081 southern Norway, based on proximal glaciofluvial stream-bank mires. *Quaternary  
1082 Science Reviews* 24, 67–90.

1083

1084 Matthews, J. A., Nesje, A., Linge, H., 2013. Relict talus-foot rock glaciers at  
1085 Øyberget, upper Ottadalen, southern Norway: Schmidt hammer exposure ages and  
1086 palaeoenvironmental implications. *Permafrost and Periglacial Processes* 24, 336–  
1087 346.

1088

1089 Matthews, J. A., Winkler, S., Wilson, P., 2014. Age and origin of ice-cored moraines  
1090 in Jotunheimen and Breheimen, southern Norway: insights from Schmidt-hammer  
1091 exposure-age dating. *Geografiska Annaler Series A, Physical Geography* 96, 531–  
1092 548.

1093

1094 Matthews, J.A., McEwen, L.J., Owen, G., 2015. Schmidt-hammer exposure-age  
1095 dating (SHD) of snow-avalanche impact ramparts in southern Norway: approaches,  
1096 results and implications for landform age, dynamics and development. *Earth Surface  
1097 Processes and Landforms* 40, 1705–1718.

1098

1099 Matthews, J. A., Owen,G., Winkler,S., Vater,A. E., Wilson,P., Mourne, R.W., Hill, J.  
1100 L., 2016. A rock-surface microweathering index from Schmidt hammer R-values and  
1101 its preliminary application to some common rock types in southern Norway. *Catena*  
1102 143, 35–44.

1103

1104 Matthews, J.A., Hill, J.L., Winkler, S., Owen, G., Vater A.E., 2018a. Autosuccession in  
1105 alpine vegetation: testing the concept on an altitudinal bioclimatic gradient,  
1106 Jotunheimen, southern Norway. *Catena* 170, 169-182.

1107

1108 Matthews, J.A., Winkler, S., Wilson, P., Tomkins, M.D., Dortch, J.M., Mourne, R.W.,  
1109 Hill, J.L., Owen, G., Vater, A.E., 2018b. Small rock-slope failures conditioned by  
1110 Holocene permafrost degradation: a new approach and conceptual model based on  
1111 Schmidt-hammer exposure-age dating, Jotunheimen, southern Norway. *Boreas* 47,  
1112 1144-1169.

1113

1114 Matsuoka, N., Murton, J., 2008. Frost weathering: recent advances and future  
1115 directions. *Permafrost and Periglacial Processes* 19, 195-210.

1116

1117 McCarroll, D., 1987. The Schmidt hammer in geomorphology: five sources of  
1118 instrument error. *British Geomorphological Research Group, Technical Bulletin* 36,  
1119 16–27.

1120

1121 McCarroll, D., 1994. The Schmidt hammer as a measure of degree of rock surface  
1122 weathering and terrain age. In: Beck, C. (Ed.), *Dating in Exposed and Surface  
1123 Contexts*. University of New Mexico Press, Albuquerque, pp29–45.

1124

1125 Mingard, K., Morrell, R., Jackson, P., Lawson, S., Patel, S., Buxton, R., 2009. Good  
1126 Practice Guide for Improving the Consistency of Particle Size Measurement. National  
1127 Physics Laboratory, Teddington [Measurement Good Practice Guide No. 111].

1128

1129 Murton, J.B., 2013. Rock weathering. In: Elias, S.A. (Ed), *Encyclopedia of Quaternary*  
1130 *Science, Volume 3*. Elsevier, Amsterdam, pp. 500-506.

1131

1132 Murton, J.B., Peterson, R., Osouf, J.-C., 2006. Bedrock fracture by ice segregation in  
1133 cold regions. *Science* 314, 1127-1129.

1134

1135 Nelson, F.E., 1998. Cryoplanation terrace orientation in Alaska. *Geografiska Annaler*  
1136 *Series A, Physical Geography* 71, 31–41.

1137

1138 Nelson, F.E., Nyland, K.E., 2017. Periglacial cirque analogues: elevation trends of  
1139 cryoplanation terraces in eastern Berigia. *Geomorphology* 293, 305-217.

1140

1141 Nesje, A., 2009. Late Pleistocene and Holocene alpine glacier fluctuations in  
1142 Scandinavia. *Quaternary Science Reviews* 28, 2119–2136.

1143

1144 Nesje, A., Dahl, S.-O., 2001. The Greenland 8200 cal. yr BP event detected in loss-  
1145 on-ignition profiles in Norwegian lacustrine sediment sequences. *Journal of*  
1146 *Quaternary Science* 16, 155–166.

1147

1148 Nesje, A., Dahl, S.O., Thun, T., Nordli, Ø., 2008. ‘Little Ice Age’ glacial expansion in  
1149 western Scandinavia: summer temperature or winter precipitation? *Climate Dynamics*  
1150 30, 789-801.

1151

1152 NIJOS, 1991. *Vegetasjonskart: Galdhøpiggen 1518 II (1:50,000)*. Norsk Institutt for  
1153 Jord og Skogkartlegging (NIJOS), Ås

1154

1155 Nyberg, R., 1991. Geomorphic processes at snowpatch sites in the Abisko Mountains,  
1156 northern Sweden. *Zeitschrift für Geomorphologie N.F.* 35, 321-343.

1157

1158 Ødegård, R.S., Sollid, J.L., Liestøl, O., 1987. *Juvflya – Kvartærgeologi og*  
1159 *geomorfologi M1:10.000*. Geografisk Institutt, Universitetet I Oslo, Oslo

1160 .

1161 Ødegård, R.S., Sollid, J.L., Liestøl, O., 1988. Periglacial forms related to terrain  
1162 parameters in Jotunheimen, southern Norway. *Permafrost: V International*  
1163 *Conference on Permafrost in Trondheim, Norway, August 1988, vol. 3*, Tapir,  
1164 Trondheim, pp. 59–61.

1165

1166 Ødegård, R.S., Sollid, J.L., Liestøl, O., 1992. Ground temperature measurements in  
1167 mountain permafrost, Jotunheimen, southern Norway. *Permafrost and Periglacial*  
1168 *Processes* 3, 231–234.

1169

1170 Ødegård, R.S., Hoelzle, M., Johanen, K.V., Sollid, J.L., 1996. Permafrost mapping  
1171 and prospecting in southern Norway. *Norsk Geografisk Tidsskrift* 50, 41–53.

1172

1173 Peltier, L.C., 1950. The geographic cycle in periglacial regions as it relates to climatic  
1174 geomorphology. *Annals of the Association of American Geographers* 40, 214-236.

1175

1176 Péwé, T.L., 1970. Altiplanation terraces of early Quaternary age near Fairbanks,  
1177 Alaska. *Acta Geographica Loziensia* 24, 357-363.

1178

1179 Powers, M.C., 1953. A new roundness scale for sedimentary particles. *Journal of*  
1180 *Sedimentary Petrology* 23, 117–119.

1181

1182 Priesnitz, K., 1988. Cryoplanation. In: Clark, M.J. (Ed.), *Advances in Periglacial*  
1183 *Geomorphology*. Wiley, Chichester, pp. 49-67.

1184

1185 Proceq, 2004. *Operating instructions. Betonprüfhammer N/NR-L/LR*. Proceq SA,  
1186 Schwerzenbach.

1187

1188 Rapp, A., 1960. Recent development of mountain slopes in Karkevagge and  
1189 surroundings, northern Scandinavia. *Geografiska Annaler* 42, 65-200.

1190

1191 Reger, R.D., 1975. Cryoplanation terraces of interior and western Alaska. PhD Thesis,  
1192 Arizona State University, Tempe, Arizona.

1193

1194 Reger, R.D., Péwé, T.L., 1976. Cryoplanation terraces: indicators of a permafrost

1195 environment. *Quaternary Research* 6, 99-109.

1196

1197 Reimer, P.J., Bard, E., Bayliss, A., Beck, J.W., Blackwell, P.G., Bronk Ramsey, C.,  
1198 Buck, C.E., Cheng, H., Edwards, R.L., Friedrich, M., Grootes, P.M., Guilderson, T.P.,  
1199 Haflidason, H., Hajdas, I., Hatté, C., Heaton, T.J., Hoffmann, D.I., Hogg, A.G.,  
1200 Hughen, A.K., Kaiser, K.F., Kromer, B., Manning, S.W., Niu, M., Reimer, R.W.,  
1201 Richards, D.A., Scott, E.M., Southon, J.R., Staff, R.A., Turney, C.S.M., van der  
1202 Plicht, A., 2013. INTCAL13 and MARINE13 radiocarbon age calibration curves 0-  
1203 50,000 years cal BP. *Radiocarbon* 55, 1869-1887.

1204

1205 Richter, H., Haase, G., Barthel, H., 1963. Die Golezterrassen. *Petermanns*  
1206 *Geographische Mitteilungen* 107, 183-192.

1207

1208 Rixhon, G., Demoulin, A., 2013. Evolution of slopes in a cold climate. In: Giardino, R.,  
1209 Harbor, J. (Eds), *Treatise on Geomorphology, Volume 8, Glacial and Periglacial*  
1210 *Geomorphology*, 392-415. Academic Press: San Diego, CA.

1211

1212 Schunke, E., 1977. Periglazialformen und formengesellschaften in der europäisch  
1213 atlantischen Arktis und Subarktis. *Abhandlungen der Akademie der Wissenschaften in*  
1214 *Göttingen, Mathematisch-Physicalische Klasse, Dritte Folge* 31, 39-62.

1215

1216 Schunke, E., Heckendorff, W.D., 1976. Resistenzstufen und kryoplanation.  
1217 Beobachtungen aus dem periglazialen Milieu Islands. *Zeitschrift für Geomorphologie*  
1218 *.Supplement Band* 24, 88-98.

1219

1220 Shakesby, R.A., Matthews, J.A., Owen, G., 2006. The Schmidt hammer as a relative-  
1221 age dating tool and its potential for calibrated age dating in Holocene glaciated  
1222 environments. *Quaternary Science Reviews* 25, 2846–2867.

1223

1224 Shakesby, R.A., Matthews, J.A., Karlén, W., Los, S., 2011. The Schmidt hammer as a  
1225 Holocene calibrated-age dating technique: testing the form of the R-value–age  
1226 relationship and defining predicted errors. *The Holocene* 21, 615–628.

1227

1228 Steiger, C., Etzelmüller, B., Westermann, S., Myhra, K.S., 2016. Modelling the  
1229 permafrost distribution in steep rock walls in Norway. *Norwegian Journal of Geology*  
1230 96, 329-341.  
1231

1232 Stroeven, A. P., Hættestrand, C., Kleman, J., Heyman, J., Fabel, D., Fredin, O.,  
1233 Goodfellow, B.W., Harbor, J. M., Jansen, J.D., Olsen, L., Caffee, M.W., Fink, D.,  
1234 Lundqvist, J., Rosqvist, G.C., Strömberg, B., Jansson, K. N., 2016: Deglaciation of  
1235 Fennoscandia. *Quaternary Science Reviews* 147, 91–121.  
1236

1237 St-Onge, D.A., 1964. Les formes de nivation de L'île Ellef Ringnes, Territoires du  
1238 Nord-Ouest. *Acta Geographica* 3, 287-304.  
1239

1240 St-Onge, D.A., 1969. Nivation landforms. *Geological Survey of Canada Paper* 69-30,  
1241 1-12.  
1242

1243 Te Punga, M.T., 1956. Altiplanation terraces in southern England. *Biuletyn*  
1244 *Peryglacjalny* 4, 331-338.  
1245

1246 Thorn, C.E., 1976. Quantitative evaluation of nivation in the Colorado Front Range.  
1247 *Geological Society of America Bulletin* 87, 1169-1178.  
1248

1249 Thorn, C.E., 1988. Nivation: a geomorphic chimera. In Clark, M.J. (ed.) *Advances in*  
1250 *Periglacial Geomorphology*, 3-31. Wiley: Chichester.  
1251

1252 Thorn, C.E., Hall, K., 1980. Nivation: an arctic-alpine comparison and reappraisal.  
1253 *Journal of Glaciology* 25, 109-124.  
1254

1255 Thorn C.E., Hall, K., 2002. Nivation and cryoplanation: the case for scrutiny and  
1256 integration. *Progress in Physical Geography* 26, 533-550.  
1257

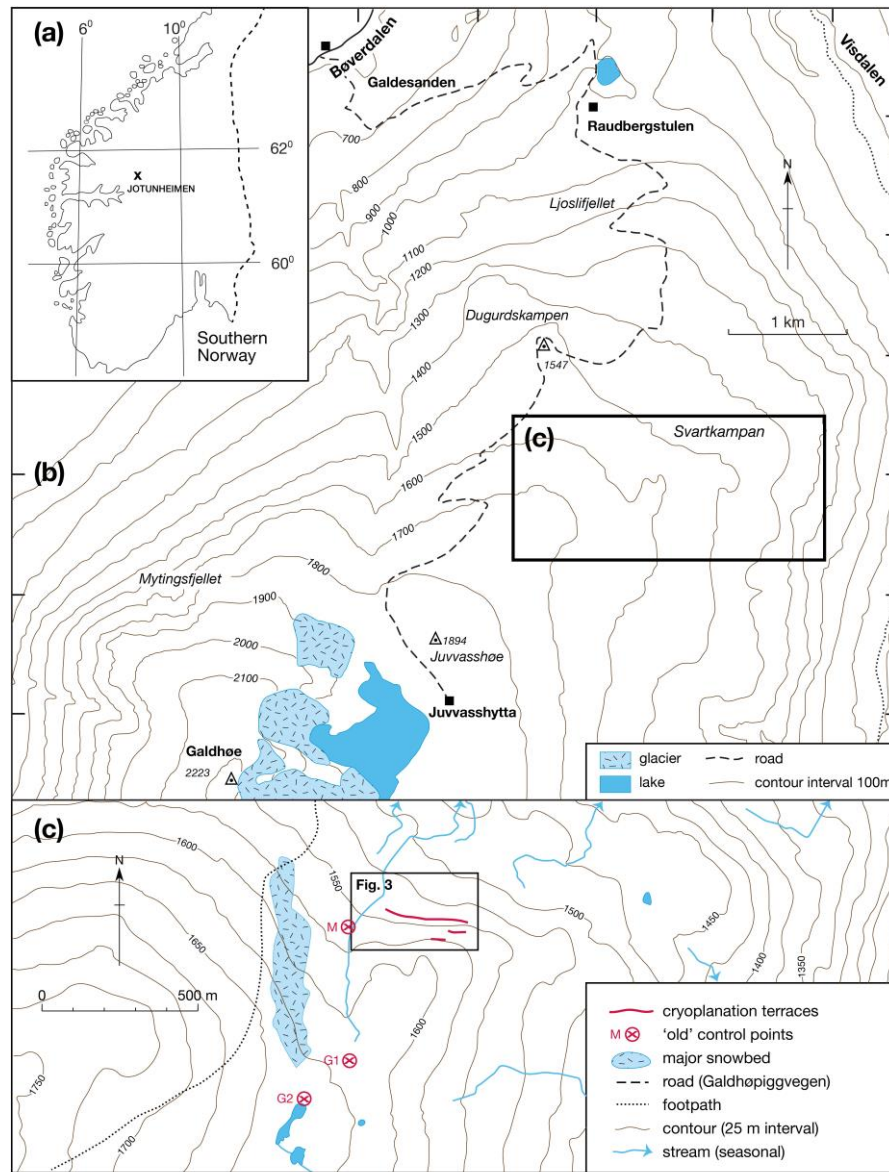
1258 Thorn, C.E., Darmody, R.G., Dixon, J.C., 2011. Rethinking weathering and  
1259 pedogenesis in alpine periglacial regions: some Scandinavian evidence. In: Martini, I.P.,  
1260 French, H.M., Pérez Albertini, A. (Eds) *Ice-marginal and periglacial processes and*  
1261 *sediments*. Geological Society of London, Special Publications 354, pp. 183-193.

1262  
1263 Traczyk, A., Migon, P., 2000. Cold-climate landform patterns in the Sudetes. Effects of  
1264 lithology, relief and glacial history. *Acta Universitatis Carolinae Geographica* 35  
1265 (Supplementum), 185-210.  
1266  
1267 Viles, H., Goudie, A., Grabb, S., Lalley, J., 2011. The use of the Schmidt hammer and  
1268 Equotip for rock hardness assessment in geomorphology and heritage science: a  
1269 comparative analysis. *Earth Surface Processes and Landforms* 36, 320–333.  
1270  
1271 Walder, J.S., Hallet, B., 1985. A theoretical model of the fracture of rock during  
1272 freezing. *Bulletin of the Geological Society of America* 96, 336-346.  
1273  
1274 Waters, R.S., 1962. Altiplanation terraces and slope development in Vest-Spitsbergen  
1275 and south-west England. *Biuletyn Peryglacjalny* 11, 89-101.  
1276  
1277 Washburn, A.L., 1979. *Geocryology: a Survey of Periglacial Processes and*  
1278 *Environments*. Arnold, London.  
1279  
1280 Wilson, P., Matthews, J.A., 2016. Age assessment and implications of late Quaternary  
1281 periglacial and paraglacial landforms on Muckish Mountain, northwest Ireland, based  
1282 on Schmidt-hammer exposure age dating (SHD). *Geomorphology* 270, 134–144.  
1283  
1284 Wilson, P., Matthews, J.A., Mourné, R.W., 2017. Relict blockstreams at Insteheia,  
1285 Valldalen-Tafjorden, southern Norway: their nature and Schmidt-hammer exposure  
1286 age. *Permafrost and Periglacial Processes* 28, 286–297.  
1287  
1288 Winkler, S., Matthews, J.A., Mourné, R.W., Wilson, P., 2016. Schmidt-hammer  
1289 exposure ages from periglacial patterned ground (sorted circles) in Jotunheimen,  
1290 Norway, and their interpretive problems. *Geografiska Annaler Series A, Physical*  
1291 *Geography* 98, 265–285.  
1292  
1293 Woo, M., 2012. *Permafrost Hydrology*. Springer, Heidelberg.  
1294  
1295



1296  
1297  
1298

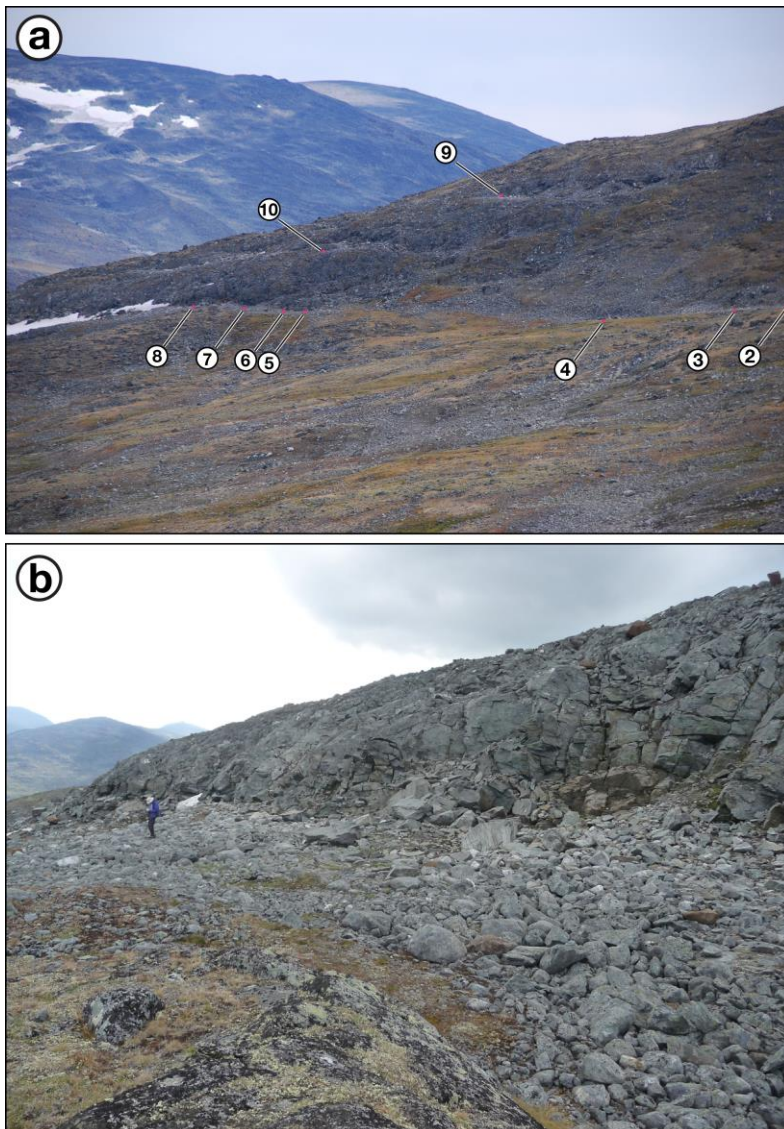
## FIGURES



1299

1300 Figure 1. (a) Location of Jotunheimen, southern Norway; (b) location of  
1301 Svartkampan, NE Jotunheimen; (c) location of the cryoplanation terraces at  
1302 Svartkampan (source: <http://www.norgeskart.no>). Sites of control points for Schmidt-  
1303 hammer exposure-age dating (M, G1 and G2; explained in the text) and location of  
1304 Figure 3 are also shown.

1305  
1306  
1307  
1308



1310

1311

1312

1313 Figure 2. (a) The sequence of cryoplanation terraces at Svartkampan viewed from the

1314 north-west (23/07/2018). Numbers indicate the positions of cross-profiles and

1315 measurement sites 2-10. Note also the late-lying snowbed at the eastern end of the

1316 main terrace (to the left of site 8) and the near-absence of snow elsewhere on this

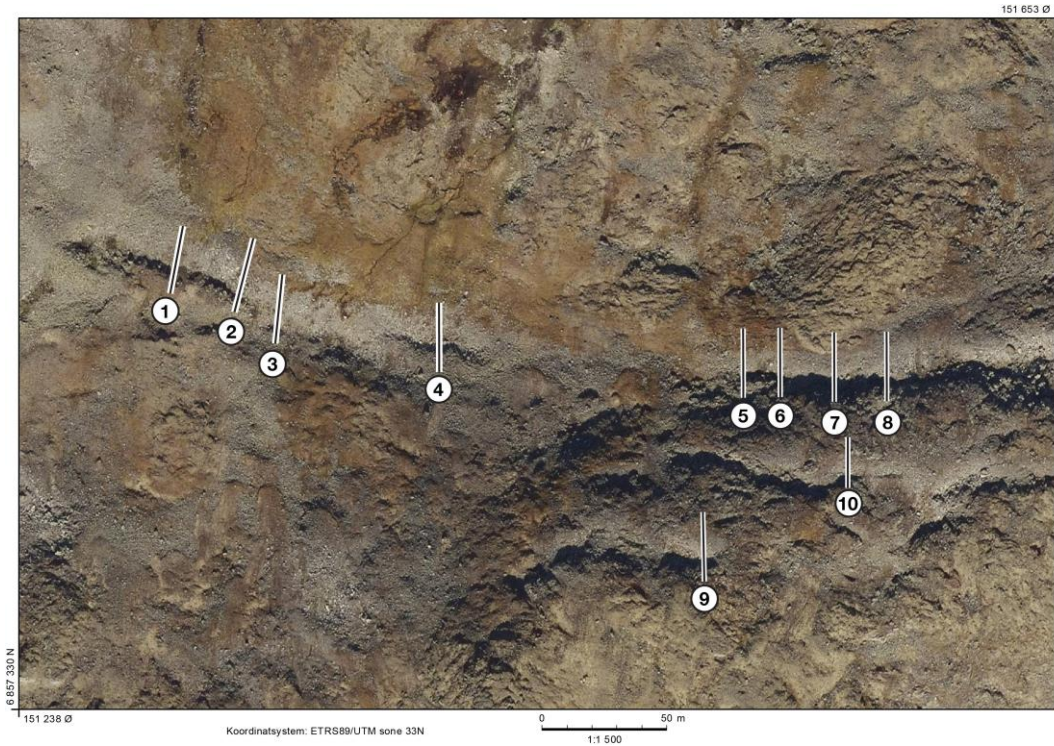
1317 terrace and on the two upper terraces (sites 9 and 10). (b) Detail of the eastern end of

1318 the main terrace (including sites 7 and 8; 22/07/2017). Note person for scale.

1319

1320

1321



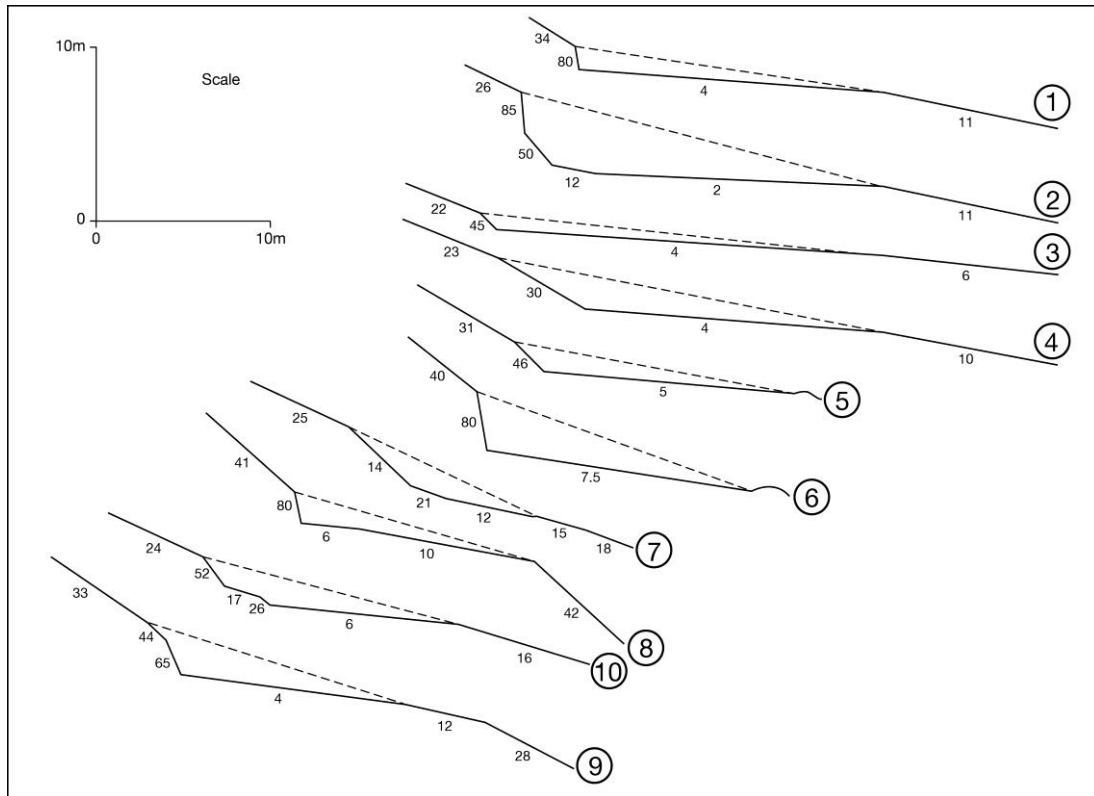
1322

1323 Figure 3. Vertical aerial photograph of the cryoplanation terraces flown on  
1324 25/09/2017 (source: <http://www.norgebilder.no>). Numbers indicate the positions of  
1325 cross-profiles and measurement sites 1-10.

1326

1327

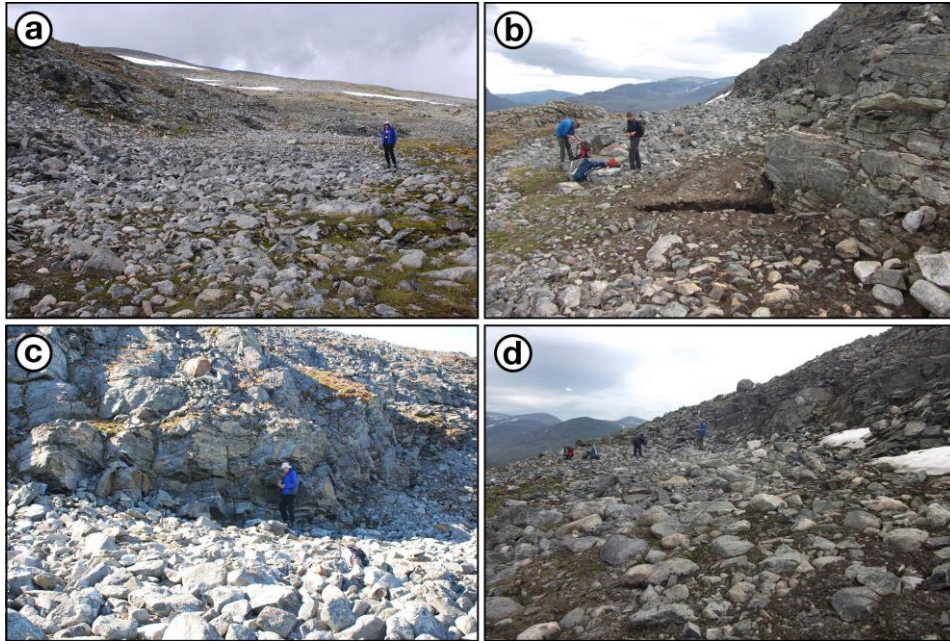
1328



1329

1330

1331 Figure 4. Cross-profiles of the cryoplanation terraces: sites 1-8 relate to the main  
1332 terrace; sites 9 and 10 are on the upper terraces. Small numbers are slope angles of the  
1333 slope segments (degrees). On each profile, the length of the terrace tread was halved  
1334 to define the inner (closest to the cliff) and outer tread. Dashed lines suggest the  
1335 volume of rock removed to form each terrace.

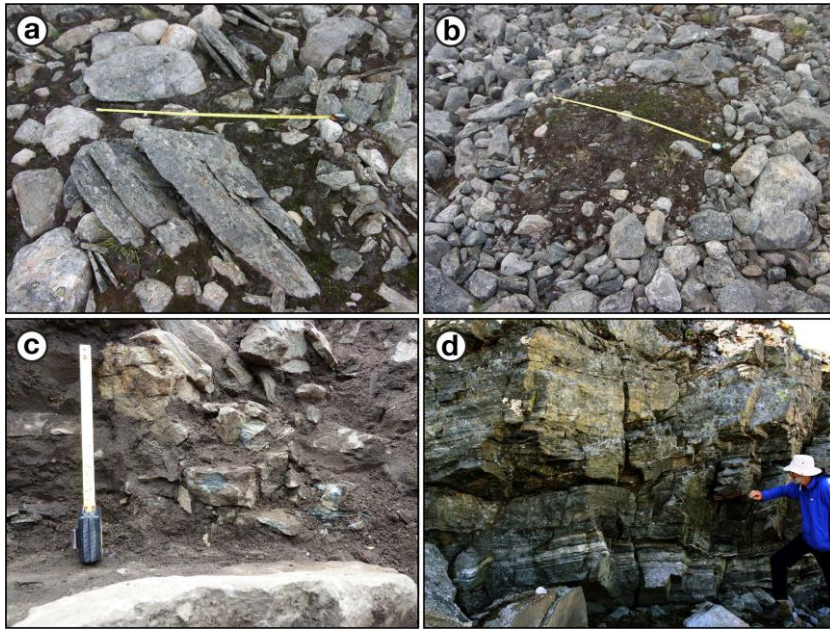


1336

1337 Figure 5. Photographs of selected cryoplanation terraces: (a) general view of sites 1-3  
1338 on the main terrace viewed from the east (30/07/2017); (b) general view of sites 6-8  
1339 on the main terrace from the north-west with excavation in the foreground  
1340 (21/07/2018); (c) site 6 from the north (21/07/2017); (d) site 10 from the west  
1341 (17/07/2018).

1342

1343

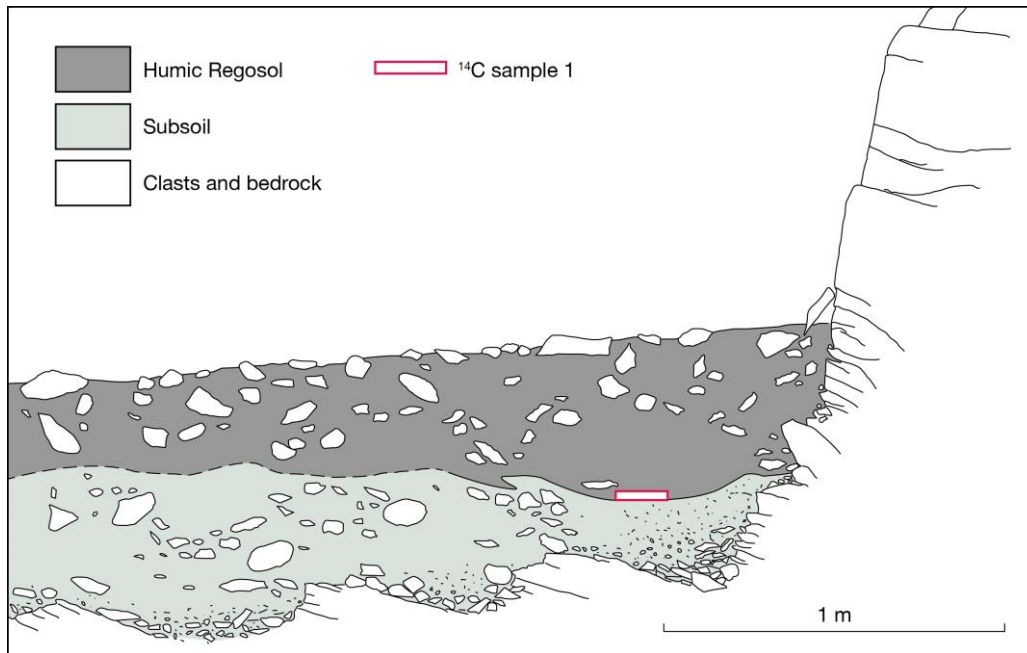


1344

1345 Figure 6. Details from cryoplanation terrace treads and cliffs: (a) sorted circle on the  
1346 terrace tread at site 2 (scale length = 1.0 m); (b) *in situ* split clasts at site 2; (c)  
1347 fractured bedrock close to the base of the cliff at site 6; (d) breccia below soil level at  
1348 the base of the cliff at the site of the excavation shown in Figure 7 (scale = 20 cm).

1349

1350



1351

1352 Figure 7. Subsurface characteristics revealed by excavation of the main cryoplanation  
1353 terrace between sites 5 and 6. Note especially the subsurface bedrock profile and the  
1354 position of the radiocarbon dating sample at the base of the Humic Regosol.

1355

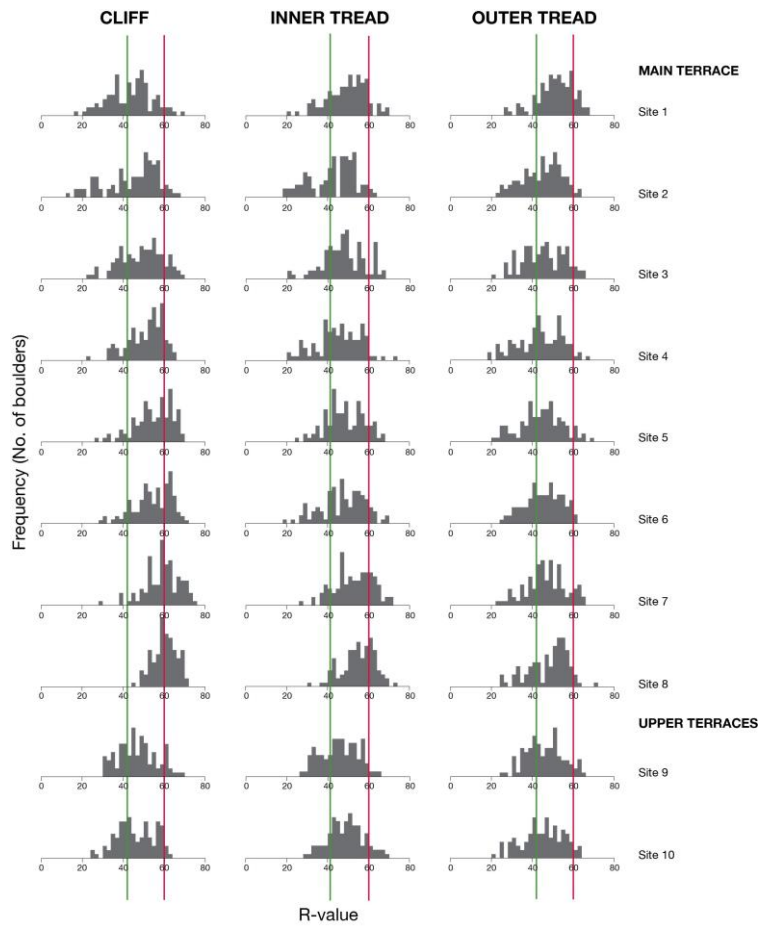
1356



1357

1358 Figure 8. Standing water at the cliff/tread junction produced by water seeping from  
1359 the cliff base near site 6 (8/07/2018).





1360

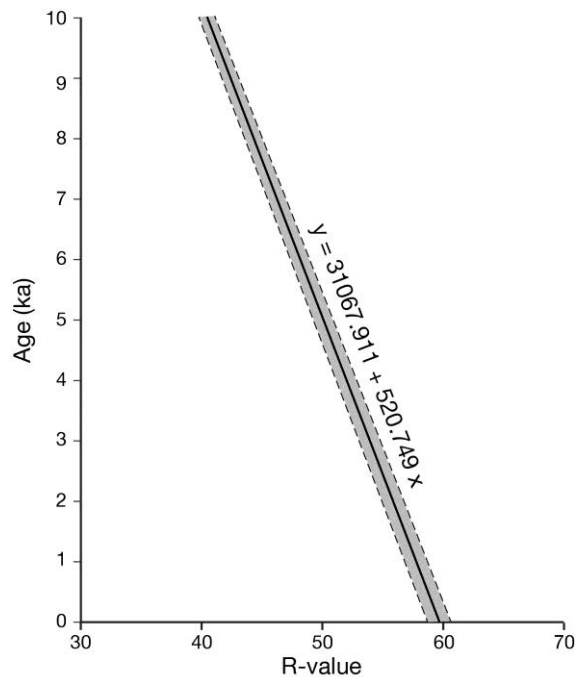
1361 Figure 9. Frequency histograms of R-values for cliffs, and for inner and outer terrace

1362 treads, from the 10 sites. Vertical lines represent mean R-values for 'old' and 'young'

1363 control points, respectively.

1364

1365



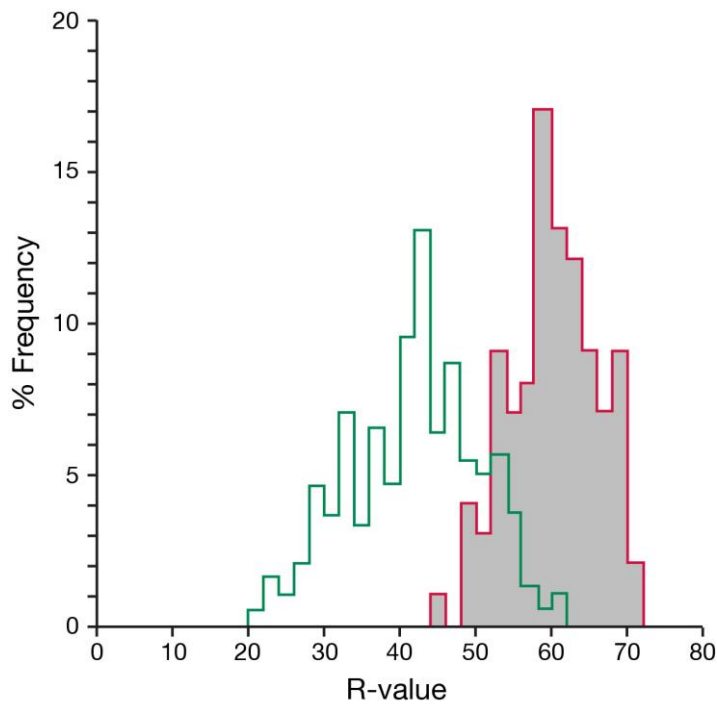
1366

1367 Figure 10. SHD calibration equation and calibration curve with 95 % confidence

1368 interval for mylonitised pyroxene-granulite gneiss at Svartkampan.

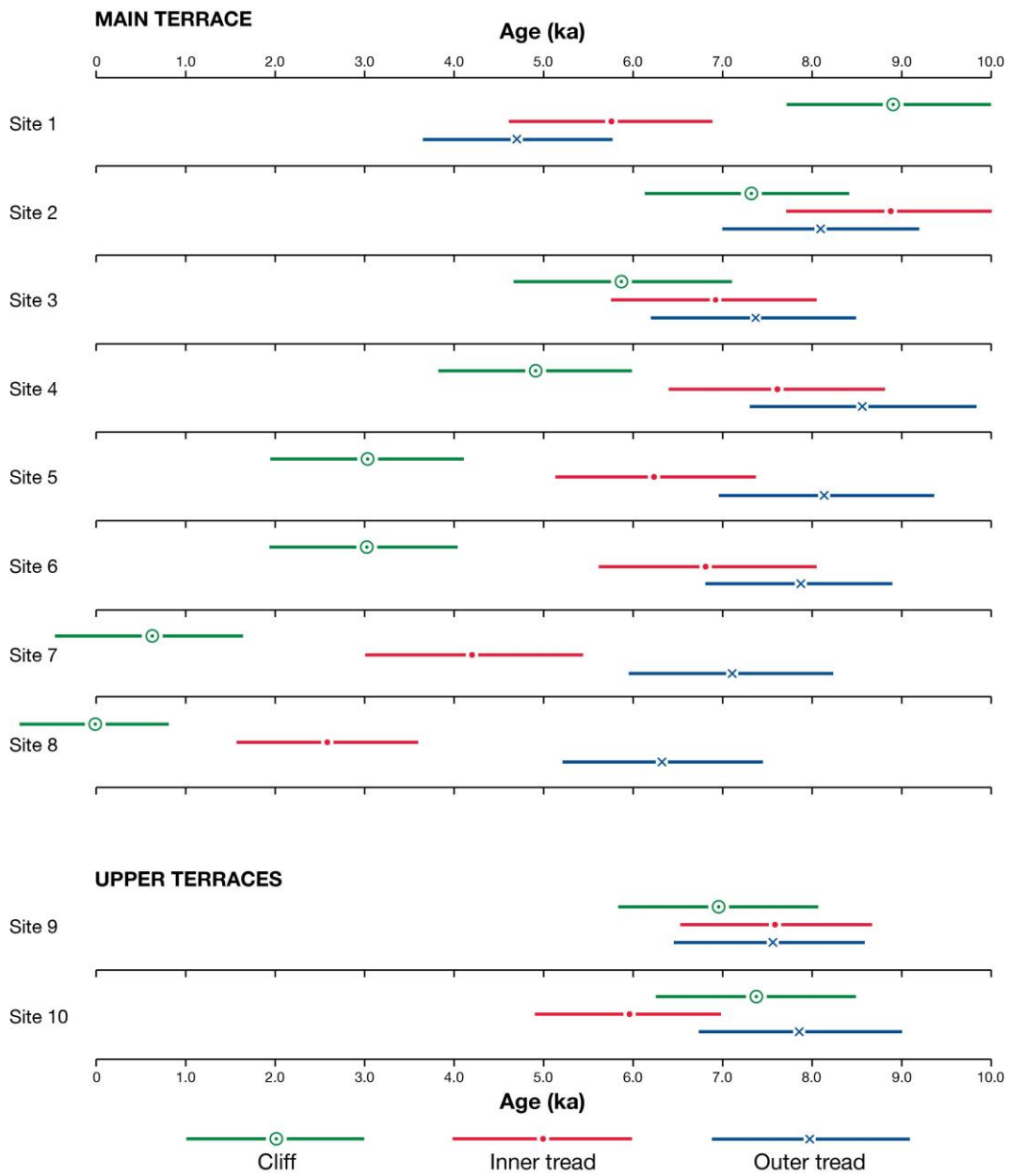
1369

1370



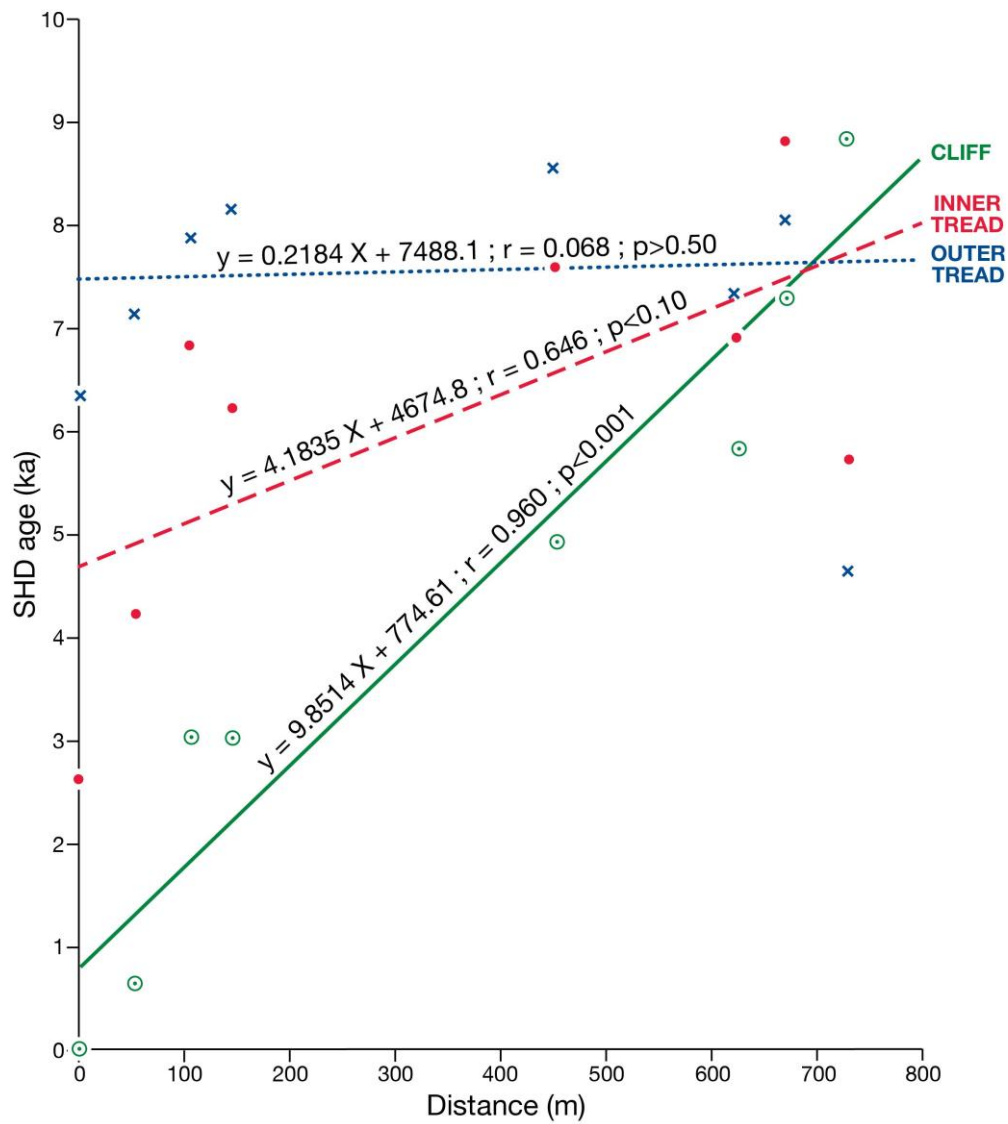
1371

1372 Figure 11. Percentage frequency histograms of R-values for the 'old' (9700 ka) and  
1373 'young' (0 ka; grey shading) control points used in this study. Note that these  
1374 symmetrical statistical distributions characteristic of single-age surfaces contrast with  
1375 most of the distributions associated with the cryoplanation terraces in Figure 8.



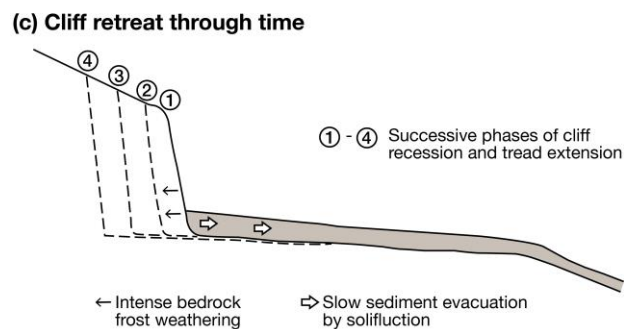
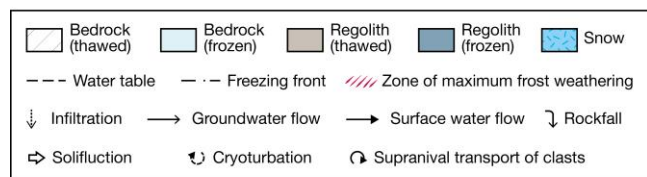
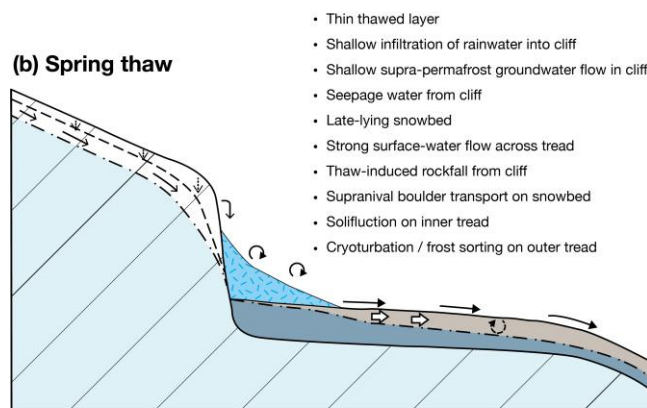
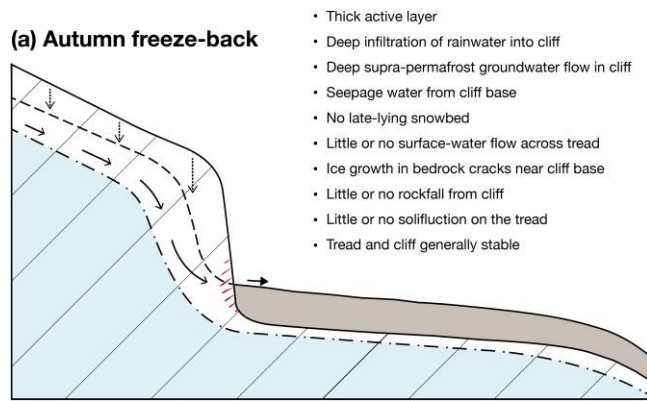
1376

1377 Figure 12. SHD ages for cliffs, inner treads and outer treads at sites from the main  
 1378 terrace (1-8) and the upper terraces (9-10). Horizontal bars are 95 % confidence  
 1379 intervals.



1380

1381 Figure 13. Linear regression analyses and correlation coefficients between SHD age  
 1382 and distance west from site 1 for cliffs, inner treads and outer treads. Note differences  
 1383 in the slope, strength and statistical significance of the relationships (n = 8 for each).



1384

1385 Figure 14. Schematic process-based model of cryoplanation terrace development:

1386 processes associated with an active cryoplanation terrace at Svartkampan during (a)

1387 autumn freeze-back (prior to the start of freezing) and (b) spring thaw (after thawing

1388 has started); (c) the developmental sequence of parallel cliff retreat due primarily to

1389 frost weathering of bedrock close to the cliff-tread junction. Note that diagonal lines in

1390 the bedrock represent the orientation of the mylonitic layering.

1391

1392 Table 1. Clast characteristics associated with terrace treads and cliffs: angular clasts include  
 1393 angular and very angular roundness categories; edge-rounded clasts include subangular,  
 1394 subrounded and rounded categories; clast size = mean size of the 25 largest clasts in angular  
 1395 or edge rounded categories ( $\pm$  95% confidence interval).

1396

---

1397	Site	Clast roundness		Clast size		Split clasts	Cliff clasts
1398	No.	(% angular)		(cm)		(%)	(% angular)
1399							
1400		Inner terrace	Outer terrace	Angular	Edge-rounded		
1401							
1402	Main terrace						
1403	1	17	10	79 $\pm$ 8	81 $\pm$ 8	3.8	56
1404	2	43	25	119 $\pm$ 6	63 $\pm$ 8	12.8	81
1405	3	27	19	83 $\pm$ 9	59 $\pm$ 9	5.3	49
1406	4	31	24	120 $\pm$ 12	73 $\pm$ 10	12.4	13
1407	5	27	12	90 $\pm$ 14	75 $\pm$ 8	5.3	87
1408	6	33	13	100 $\pm$ 12	68 $\pm$ 7	5.9	86
1409	7	31	19	95 $\pm$ 8	70 $\pm$ 8	4.0	77
1410	8	77	35	116 $\pm$ 15	68 $\pm$ 8	5.5	97
1411	Upper terraces						
1412	9	14	7	81 $\pm$ 5	90 $\pm$ 8	3.1	82
1413	10	17	5	90 $\pm$ 14	94 $\pm$ 9	4.8	92
1414							
1415							
1416							
1417							

---

1418 Table 2. Schmidt-hammer R-values from cryoplanation terraces (surface boulders) and  
 1419 associated bedrock cliffs: s = standard deviation; CI = 95% confidence interval; n = 100  
 1420 impacts.

1421	<hr/>									
1422	Transect	Cliff			Inner terrace			Outer terrace		
1423	No.	<hr/>			<hr/>			<hr/>		
1424		Mean	s	CI	Mean	s	CI	Mean	s	CI
1425	<hr/>									
1426	Main terrace									
1427	1	42.59	10.27	2.26	48.66	9.40	2.07	50.66	8.72	1.92
1428	2	45.62	10.47	2.31	42.59	10.36	2.28	44.16	9.40	2.07
1429	3	48.36	10.47	2.31	46.38	9.35	2.06	45.53	9.87	2.18
1430	4	50.22	9.01	1.99	45.05	10.48	2.31	43.19	11.16	2.46
1431	5	53.86	8.91	1.96	47.66	9.16	2.02	43.95	10.55	2.33
1432	6	53.79	9.28	2.05	46.51	10.77	2.37	44.50	9.08	2.00
1433	7	58.45	8.45	1.86	51.54	10.37	2.29	45.96	9.71	2.14
1434	8	59.66	5.62	1.24	54.66	7.84	1.73	47.47	9.55	2.10
1435	Upper terraces									
1436	9	46.52	9.53	2.10	45.10	9.07	2.00	45.24	8.98	1.98
1437	10	45.52	9.23	2.04	48.25	8.55	1.89	44.58	9.66	2.13
1438	<hr/>									
1439										
1440										
1441										



1442 Table 3. Schmidt-hammer R-values from local control-point surfaces of known age: s =  
 1443 standard deviation; CI = 95% confidence interval; n = No. of impacts; age of old control  
 1444 points = 9700 years; age of young control points = 0-50 years; M = mylonitised pyroxene-  
 1445 granulite gneiss; G = pyroxene-granulite gneiss.

---

1447 1448 1449 1450	Lithology	Old control point				Young control point				Source
		Mean	s	CI	n	Mean	s	CI	n	
1451	M	41.03	8.57	0.98	300	59.66	5.62	1.12	100	This study
1452	G1	42.42	9.04	0.94	355	-	-	-	-	This study
1453	G2	38.59	9.16	0.96	350	-	-	-	-	This study
1454	G3	38.04	11.49	1.43	250	57.31	8.25	1.03	250	Matthews et al. (2014)

---

1455  
 1456  
 1457  
 1458

1459 Table 4. Schmidt-hammer exposure-ages (years) from cryoplanation terraces and associated  
 1460 cliffs: SHD age = mean age  $\pm$  95% confidence intervals of surface boulders or bedrock cliffs;  
 1461 Cs and Cc are the error components used to calculate the confidence intervals (see text). All  
 1462 ages are rounded to the nearest 5 years.

1463	<hr/>									
1464	Transect	Cliff			Inner terrace			Outer terrace		
1465	No.	<hr/>			<hr/>			<hr/>		
1466		SHD age	Cs	Cc	SHD age	Cs	Cc	SHD age	Cs	Cc
1467	<hr/>									
1468	Main terrace									
1469	1	8890 $\pm$ 1185	1065	515	5730 $\pm$ 1115	975	540	4690 $\pm$ 1025	865	545
1470	2	7310 $\pm$ 1210	1085	525	8890 $\pm$ 1195	1075	515	8070 $\pm$ 1105	975	520
1471	3	5885 $\pm$ 1215	1085	535	6915 $\pm$ 1105	970	530	7360 $\pm$ 1150	1025	525
1472	4	4915 $\pm$ 1080	935	545	7610 $\pm$ 1210	1085	525	8575 $\pm$ 1270	1160	515
1473	5	3020 $\pm$ 1080	925	560	6250 $\pm$ 1090	950	535	8180 $\pm$ 1215	1095	520
1474	6	3055 $\pm$ 1115	965	560	6850 $\pm$ 1235	1120	530	7895 $\pm$ 1080	945	520
1475	7	630 $\pm$ 1050	875	580	4230 $\pm$ 1210	1075	550	7135 $\pm$ 1140	1010	530
1476	8	0 $\pm$ 825	585	585	2605 $\pm$ 1000	815	585	6350 $\pm$ 1125	990	535
1477	Upper terraces									
1478	9	6845 $\pm$ 1120	990	530	7580 $\pm$ 1080	940	535	7510 $\pm$ 1070	930	525
1479	10	7365 $\pm$ 1095	960	525	5940 $\pm$ 1040	890	535	7855 $\pm$ 1130	1005	520
1480	<hr/>									

1481  
 1482  
 1483

1484 Table 5. Radiocarbon dates from the main terrace at Svartkampan. Depth = depth from the  
 1485 terrace surface; distance = distance from the bedrock cliff base.

1486

---

1487	Lab.	Sample	Depth	Distance	<sup>14</sup> C age	δ <sup>13</sup> C	Calibrated age range
1488	No.	No.	(cm)	(cm)	(yr BP)	(‰)	(cal. yr BP; 2σ)
1490	Beta-501707	1.1	45-43	50	3630 ± 30	-24.0	4076-3854
1491	Beta-501708	1.2	42-40	60	4130 ± 30	-24.1	4821-4532
1492	Beta-501709	2.1	60-58	30	3030 ± 30	-24.8	3345-3084

---

1493

1494

1495

1496